Generative Modelling of Lévy Area for High Order SDE Simulation

Andraž Jelinčič[*]
Department of Mathematical Sciences
University of Bath
aj2382@bath.ac.uk

Jiajie Tao[*]
Department of Mathematics
University College London
jiajie.tao.21@ucl.ac.uk

William F. Turner[*]
Department of Mathematics
Imperial College London
william.turner17@imperial.ac.uk

Thomas Cass
Department of Mathematics
Imperial College London
thomas.cass@imperial.ac.uk

James Foster
Department of Mathematical Sciences
University of Bath
jmf68@bath.ac.uk

Hao Ni
Department of Mathematics
University College London
h.ni@ucl.ac.uk

Abstract

It is well understood that, when numerically simulating SDEs with general noise, achieving a strong convergence rate better than $O(\sqrt{h})$ (where h is the step-size) requires the use of certain iterated integrals of Brownian motion, commonly referred to as its "Lévy areas". However, these stochastic integrals are difficult to simulate due to their non-Gaussian nature and for a d-dimensional Brownian motion with $d > 2$, no fast almost-exact sampling algorithm is known.

In this paper, we propose LévyGAN, a deep-learning-based model for generating approximate samples of Lévy area conditional on a Brownian increment. Due to our "Bridge-flipping" operation, the output samples match all joint and conditional odd moments exactly. Our generator employs a tailored GNN-inspired architecture, which enforces the correct dependency structure between the output distribution and the conditioning variable. Furthermore, we incorporate a mathematically principled characteristic-function based discriminator. Lastly, we introduce a novel training mechanism termed "Chen-training", which circumvents the need for expensive-to-generate training data-sets. This new training procedure is underpinned by our two main theoretical results.

For 4-dimensional Brownian motion, we show that LévyGAN exhibits state-of-the-art performance across several metrics which measure both the joint and marginal distributions. We conclude with a numerical experiment on the log-Heston model, a popular SDE in mathematical finance, demonstrating that high-quality synthetic Lévy area can lead to high order weak convergence and variance reduction when using multilevel Monte Carlo (MLMC).

---

[*]Equal contribution.

1 Introduction

The numerical simulation of Stochastic Differential Equations (SDEs) is a ubiquitous task encountered in a wide variety of fields, ranging from mathematical finance [Shr04] and systems biology [Bro+20] to molecular dynamics [LM15] and data science [Li+19]. Real-world phenomena arising in these areas are often described well by SDEs formulated through *Itô calculus* and of the general form:

$$dX_t = f(X_t)dt + \sum_{i=1}^{d} g_i(X_t)dW_t^{(i)}, \quad X_0 = x_0, \tag{1}$$

where the solution $X = \{X_t\}_{t \in [0,T]}$ takes values in $\mathbb{R}^e$, $W = (W^{(1)}, \ldots, W^{(d)})$ denotes a standard d-dimensional Brownian motion and $f, g_i : \mathbb{R}^e \to \mathbb{R}^e$ are suitably regular vector fields on $\mathbb{R}^e$. In practice, one is often concerned with estimating quantities of the form $\bar{\varphi} := \mathbb{E}\left[\varphi(X) \mid X_0 = x_0\right]$, where the function φ may depend on the whole trajectory of X or simply on the terminal value X_T; such as the payoff of a European call-option. On occasion, it may be possible to obtain $\bar{\varphi}$ by solving certain PDEs (e.g. through the backward Kolmogorov equation or the Feynman-Kac formula).

However, the standard approach is to use Monte Carlo simulation, where one uses a discretisation scheme to generate approximate sample paths $\{\widehat{X}_i\}_{i=1}^N$ of X, which can be used to approximate $\bar{\varphi}$ by taking the average of $\{\varphi(\widehat{X}_i)\}_{i=1}^N$. Given the importance of Monte Carlo simulation in applications, there is a rich literature concerning numerical methods for SDEs and their theoretical properties. A broad range of discretisation schemes are available, such as the classical Euler-Maruyama and Milstein schemes as well as the higher order Talay [Tal90] and Ninomiya-Victoir [NV08] schemes. For more details on the numerical simulation of SDEs, we refer the reader to [KP92] and [PT85].

There are two standard measures for the effectiveness of numerical schemes: strong error (or MSE) and weak error. It is a well-known result of Clark and Cameron [CC80] that numerical schemes using only increments of Brownian motion are limited in general to a strong convergence rate of at most $O(\sqrt{h})$, where h denotes the step size. Furthermore, to the best of our knowledge, all numerical schemes achieving second order weak convergence require the generation of random variables in addition to the Brownian increments. In particular, the Talay scheme [Tal90] and the Ninomiya-Victoir scheme [NV08] require the generation of Rademacher random variables. Further examples include the Ninomiya-Ninomiya scheme [NN09] and a stochastic Runge-Kutta method due to Rößler [Röß09]. In all of these cases, the additional random variable(s) are generated to replace certain second order iterated integrals of Brownian motion, which are commonly referred to as its *Lévy area*.

Definition 1.1. The Lévy area of a d-dimensional Brownian motion over $[s, t]$ is a $d \times d$ antisymmetric matrix whose (i, j)-th entry is entries given by,

$$A_{s,t}^{(i,j)} := \frac{1}{2}\left(\int_s^t (W_r^{(i)} - W_s^{(i)})\,dW_r^{(j)} - \int_s^t (W_r^{(j)} - W_s^{(j)})\,dW_r^{(i)}\right).$$
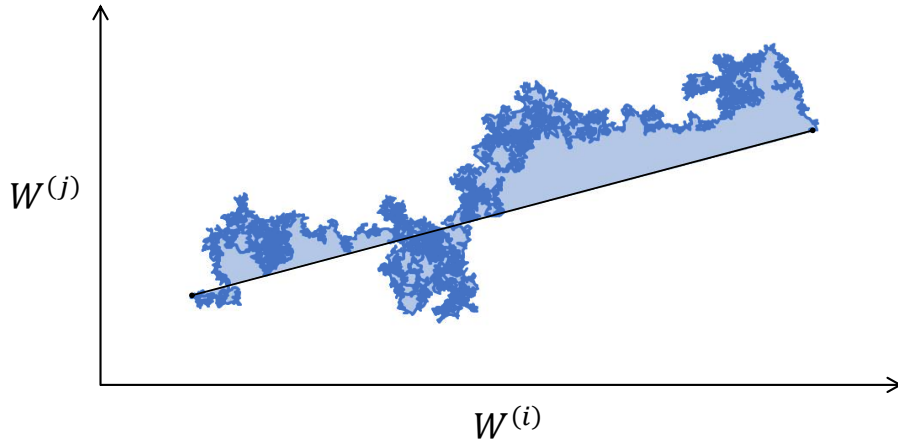

Figure 1: Each entry $A^{(i,j)}$ is the area between the independent Brownian motions $W^{(i)}$ and $W^{(j)}$ (diagram adapted from [Fos20]).

When the vector fields of the SDE Equation (1) do not satisfy the commutativity condition $[g_i, g_j] = 0$ (where $[g_i, g_j](x) := g_j'(x)g_i(x) - g_i'(x)g_j(x)$ denotes the standard Lie bracket of vector fields), then schemes that achieve high order Strong convergence, such as the Milstein and log-ODE methods, require the simulation of Lévy area. Consequently, the approximation of Lévy area has received much interest in recent decades, with the view towards both high order weak and strong convergence.

Approximations to Lévy area have been well studied [Dav14; Dic07; GL94; KP92; KPW92; Fos20; FH22; MR22; MW14; Wik01], with the majority of approximations concerning strong estimation. Strong estimators aim to approximate Lévy area by minimising the mean-squared error so that the resulting estimator may be incorporated into the strong analysis of the discretisation scheme. Typically such estimators rely on truncated expansions of Brownian motion, such as the Fourier series expansion [KP92; KPW92; KR23], the Karhunen-Loève expansion [Loè78] and more recently the polynomial expansion [Fos25; FH22; FLO20]. These estimators are often improved by estimating the tail sum of the of the expansion in an appropriate manner, see for example [MR22; Wik01].

To the best of our knowledge, there is no known scheme which simulates Lévy area exactly, with even the "rectangle-wedge-tail" algorithm of Gaines and Lyons [GL94] requiring numerical integration. Moreover, this approach is only applicable in $d = 2$. On the other hand, the main drawback of the truncated expansion methods is the cost of simulation. In practice, one is often required to generate millions of Lévy area samples, and the aforementioned methods often require a high truncation level to achieve good performance. Consequently, in recent years, there has been a renewed focus on approximations of Lévy area that are suitable for weak discretisation schemes, where the estimator is less costly to generate. The aim of a weak estimator is to match some moments of the Lévy area given a Brownian increment. These estimators differ in complexity depending on their intended usage. Basic estimators include the Rademacher random variables that appear in the Talay scheme [Tal90] and Davie's approximation [Dav14; FL15] which uses a Gaussian random variable with the correct variance (this may be improved to have the correct conditional variance given the Brownian increment [Fos20]). Perhaps the most sophisticated weak approximation is due to Foster [Fos20], which matches the first five conditional moments of Lévy area given the Brownian increment when $d \leq 3$.

In this article, we provide a new approach to the construction of weak estimators of Lévy area given a Brownian increment through the use generative modelling techniques. To the best of our knowledge, this is the first time that the powerful toolkits provided by modern machine learning have been applied to the problem of Lévy area simulation. Arguably the main obstacle to this approach is the computation effort required to generate considerable amounts of precise samples of Lévy area. We note this is in principle possible, through the use of a truncated Fourier series method [KR23], with other options also possible. However, in the context of Lévy area generation, we present a novel training algorithm based on Chen's relation [Che57] that allows for the training of a generative model without access to a dataset of Lévy area samples.

1.1 Our contributions

In this article we present LévyGAN, a deep-learning based generative model that simulates the Lévy area of arbitrary dimensional Brownian motions. Deep-learning based generative models have been widely used for data synthesis where a parametric model is trained to learn the target distribution. Among the variety of generative models, GAN-typed models [MO14], [Goo+14] have been particularly noteworthy for their performances. GAN, short for Generative Adversarial Network, operates on the compelling principle of adversarial training. This approach consists of two neural networks - a generator and a discriminator - that are trained simultaneously. The generator's task is to create synthetic data, while the discriminator's role is to distinguish between real and generated data.

With no exception, GAN-type models also possess drawbacks like other generative models. The necessity of real data as reference sets for training is one of them. Machine learning models are often data-driven and sometimes data-greedy; normally, practitioners collect real-world data and approximate its distribution using an empirical distribution outputed by the generator. This is especially pertinent in the context of Lévy area generation, where a competitive method needs to achieve very high accuracy, which incurs a high statistical complexity, and thus requires large amounts of data. In contrast to standard GANs, score-based diffusion models and variational autoencoders, LévyGAN is designed to learn the target distribution without requiring any samples from it at all. We

term this approach "Chen-training", which is theoretically underpinned by the unique invariance of the joint law of Brownian motion and Lévy area under Chen's relation, see Theorem 4.5.

We have designed both the generator and discriminator by exploring the features of the joint law of Brownian motion and its Lévy Area [FH22; FLO20; Fos20]. In particular, for the generator, we ensure that the joint distribution of our generator is permutation invariant and that each component of the generated area depends only on the relevant components of the Brownian increment. We also ensure that all odd cross moments of our generator are exact through the multiplication by certain Rademacher random variables. For the discriminator, we have chosen a characteristic function based discriminator, initially proposed in [FSS20; Li+20a]. Inspired by this approach and the more general method of [LLN23], we define the unitary characteristic function of a random variable as a generalization of the characteristic function onto higher degree Lie algebra.

For our numerical results, we train the LévyGAN in $d = 4$. It is noteworthy that the model is able to generate the Lévy area for arbitrary Brownian dimensions, with no loss in performance guaranteed in $d' < d$ and empirically strong performance for $d' > d$. Empirically, we show that LévyGAN attained the best performance among other weak estimators, such as those found in [Dav14] and [Fos20], in terms of distributional metrics and is comparable in generation speed to the method in [Fos20]. Finally we provide an application of weak approximations to Lévy area to high order multi-level Monte Carlo numerical schemes. In this example, we demonstrate that the inclusion of an approximate Lévy area term in the Strang splitting method achieves higher order variance reduction and weak convergence. Moreover, we provide evidence that an estimator that only matches the variance of Lévy area (such as the Rademacher random variables found in the Talay scheme) is not appropriate for this application. The LévyGAN implementation, together with a trained model for $d = 4$ can be found at github.com/andyElking/LevyGAN.

1.2 Outline and Common Notation

This article is divided into five main sections. In Section 2 we recall the standard setup of generative adversarial networks and discuss why the traditional approach to generative modelling is not easily applicable to our setting. In Section 3 we outline the structure of our generator. This section focuses on the symmetries of the joint law of Brownian motion and Lévy area that we hard code into our generator. This includes so-called "bridge-flipping", a precise multiplication by certain Rademacher random variables to ensure all joint odd moments are correctly estimated and to help the generator train evenly across all quadrants in space. In Section 3.2 we introduce a network architecture dubbed "pair-net" inspired by graph neural networks that ensures the correct dependence structure between the coordinates of Brownian motion and the coordinates of Lévy area. The structure of our discriminator is outlined in Section 4. Here we discuss two alternatives for a loss function based on the analytical form of the joint characteristic function of Lévy area and Brownian motion and a generalisation termed the unitary characteristic function proposed in [LLN23]. Our novel training approach "Chen-training" is covered in Section 4.2, before the whole training procedure is summarised in Section 5. Finally, in Section 6, we compare the distributional performance of our generator in comparison to the state-of-the-art Foster method [Fos20] and demonstrate the applicability of weak estimators for Lévy area to multilevel Monte-Carlo.

To conclude the introduction, we outline some common notation to be used throughout the article.

1) $\mathbb{P}_{X|Y=y}$ for the conditional distribution of X given $Y = y$.

2) With abuse of notation $(X \mid Y = y) \overset{d}{=} (Z \mid Y = y)$ if $\mathbb{P}_{X|Y=y} = \mathbb{P}_{Z|Y=y}$.

3) $(W_t)_{t\in[0,1]}$ for a d-dimensional Brownian motion, and the process $(A_t)_{t\in[0,1]}$ with $A_t = \left\{ A_t^{(i,j)} \right\}_{1 \le i < j \le d}$ a $\frac{d(d-1)}{2}$-dimensional vector representing the flattened upper triangle of the Lévy area matrix associated with the Brownian motion. Unless stated otherwise, we denote by a the dimension of Lévy area, i.e. $a = \frac{d(d-1)}{2}$.

4) For any process $(X_t)_{t\in[0,1]}$, X_t denotes the process evaluated at time t.

5) $\mathbb{P}_{(W_t, A_t)}$ for the joint law of Brownian motion and Lévy area at time t.

6) $\mathcal{N}^d(\mu, \sigma^2)$ for a d-dimensional Gaussian distribution with independent coordinates, each with mean μ and variance σ^2.

7) $\text{Rad}^d(p)$ for a d-dimensional Rademacher random variable with independent entries each of which takes 1 and -1 with probability p and $1 - p$ respectively.

8) Φ_X for the characteristic function of a random variable X.

9) $W_{s,t} \coloneqq W_t - W_s$ for the increments of a Brownian motion $(W_t)_{t \in [0,1]}$, and we use $W_t = W_{0,t}$ interchangeably.

10) For any *tensor*, i.e. an element $\mathbf{x} \in \mathbb{R}^{\cdot \times d}$, we always denote by $x^{(i)} \in \mathbb{R}^{\cdot}$ the ith coordinate of the second dimension.

2   The GAN Architecture

The goal of this article is to build an efficient and accurate estimator that approximates the conditional law $\mathbb{P}_{A_t | W_t}$, and hence the joint law, $\mathbb{P}_{(W_t, A_t)}$, of a Brownian increment and its Lévy area. Thanks to the scaling property of Brownian motion, it is enough to consider the problem when $t = 1$.

We adopt a conditional GAN (Generative Adversarial Network) approach as proposed by [MO14]. GAN-typed models, initially proposed by [Goo+14] consist of a pair of competing neural networks - the generator and the discriminator. The aim of the generator is to create "fake" data $\widetilde{\mathbf{x}}$, from some noise distribution, trying to mimic a target distribution, while the discriminator will be given both $\widetilde{\mathbf{x}}$ and data $\mathbf{x}$ from the true distribution and will try to distinguish the ground truth between them. The dynamics between the generator and discriminator are controlled by a min-max game acting on a loss function, which usually represents the distance between two distributions. In a conditional GAN, the generator is given not only samples from the noise distribution, but also the conditioning variable – in our case, this is the Brownian increment W, or later the space-time Lévy area H (see Section 3.1). Here we provide the description of a classical conditional GAN adapted to our interest.

Definition 2.1 (Classical conditional GAN for Lévy Area generation). Let $d \geq 2$ be the Brownian dimension, and $a \coloneqq \frac{d(d-1)}{2}$ be the dimension of the associated Lévy area vector. Assume z is an n-dimensional noise vector distributed according to $\mathbb{P}_z$. The conditional generator G_θ and the discriminator D_η are maps

$$G_\theta : \mathbb{R}^d \times \mathbb{R}^n \to \mathbb{R}^d \times \mathbb{R}^a \quad D_\eta : \mathbb{R}^d \times \mathbb{R}^a \to \mathbb{R},$$

that are parametrized by θ and η respectively. When restricted to the first d-coordinates of the domain and co-domain, G_θ is enforced to be identity, i.e. $G_\theta(w, z) = (w, \widetilde{A})$. Let $\mathbb{P}_{(W_1, A_1)}$ be the ground truth distribution of the coupled process. An example loss function might be given by

$$L(\theta, \eta) \coloneqq \mathbb{E}_{(w,A) \sim \mathbb{P}_{(W_1,A_1)}} \left[D_\eta(w, A) \right] - \mathbb{E}_{w \sim \mathbb{P}_{W_1}, z \sim \mathbb{P}_z} \left[D_\eta(G_\theta(w, z)) \right],$$

where one restricts D_η to be at most 1-Lipschitz. The models are trained using the min-max game $\min_\theta \max_\eta L(\theta, \eta)$ until convergence. The generator obtained is then used to simulate Lévy areas.

Since there are no known methods for exact simulation of Lévy areas in $d > 2$, the "true" Lévy area samples $\mathbf{A} \sim \mathbb{P}_{A_1 | W_1}$ must themselves be obtained through approximate simulation. In particular, we might generate the "true" Lévy area samples using a Julia-language package created by [KR23], which complements their paper about approximate strong simulation of Lévy area through truncated Fourier series methods. We also present the flowchart of this methodology in Figure 2.
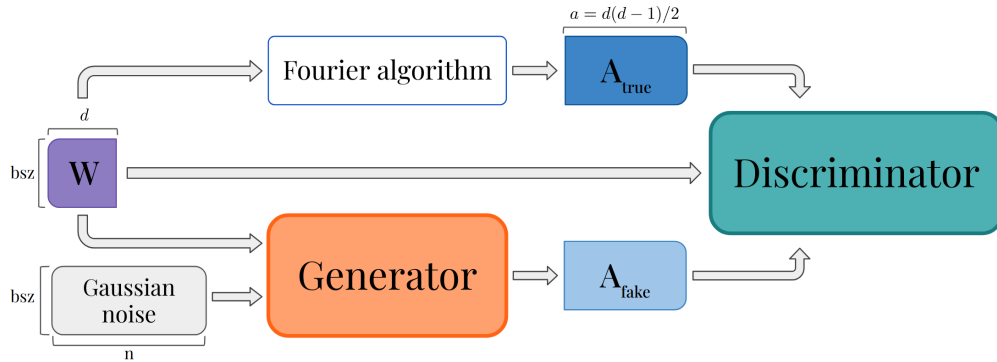

Figure 2: A schematic of Lévy generation for classical conditional GAN. Throughout this article, `bsz` represents the training batch-size.

5

The main drawback of this methodology is the need for simulating approximate real samples of Lévy area. Using real data not only slows the training procedure but also introduces simulation error (due to the truncation in the Fourier series) and finite sample error (leading to overfitting). In order to address this problem, we propose a novel approach, LévyGAN, which completely excludes real samples from the training process and is well justified by our two main theoretical contributions Theorem 4.5 and Theorem B.4.

3 Generator

In order to improve the accuracy of the generated distribution we can consider the symmetries of the Lévy area distribution and hard-code them into the generator itself. This way the generator will consist of both a neural net, and additional operations applied to the network's output. One symmetry of Lévy area that is desirable to reflect is the fact that its distribution is mean zero when conditioned on any increment $W_{0,1} = w$. We do this through two operations, which combined we term "bridge-flipping".

3.1 Bridge-Flipping

We would like to hard-code the symmetry of Lévy area about zero into the generator's architecture. Even though each dimension of Lévy area $A^{(i,j)}$ is symmetric about zero, their joint distribution is not invariant to multiplying any individual dimension by -1. The dimensions of the underlying Brownian motion, however, are independent, and hence each can be mirrored separately without violating their joint law.

The goal is hence to find a symmetry of Lévy area corresponding to independently flipping individual dimensions of the Brownian motion. Notice, however, that we are trying to generate Lévy area conditional on a fixed input $W_{0,1} = w$, and so we do not wish to flip the increment of Brownian motion itself. We can circumvent this issue by considering the polynomial expansion of Lévy area [FH22], which decomposes the Brownian motion into the components dependent on w and components independent of w, the latter of which can then be flipped independently. To this end, we first define the Brownian bridge and its accompanying "space-time" and "space-space" Lévy areas.

Definition 3.1 (Brownian bridge). Let $0 \leq s \leq t < \infty$. Then the Brownian bridge of W on $[s, t]$ returning to zero at time t is defined as

$$B_{s,u} := W_{s,u} - \frac{u-s}{t-s} W_{s,t} \quad \text{for } u \in [s, t].$$

The "space-time" Lévy area $H_{s,t} \in \mathbb{R}^d$ and "space-space" Lévy area $b_{s,t} \in \mathbb{R}^{d \times d}$ of B over $[s, t]$ are

$$H_{s,t}^{(i)} := \frac{1}{t-s} \int_s^t B_{s,u}^{(i)} \, du = \frac{1}{t-s} \int_s^t W_{s,u}^{(i)} - \frac{u-s}{t-s} W_{s,t}^{(i)} \, du \quad \text{for } 1 \leq i \leq d, \qquad (2)$$

$$b_{s,t}^{(i,j)} := \int_s^t B_{s,u}^{(i)} \circ dB_u^{(j)} \quad \text{for } 1 \leq i, j \leq d. \qquad (3)$$

Whenever $s = t$, we define $b_{s,t} = H_{s,t} = 0$. We write H_t and b_t for $H_{0,t}$ and $b_{0,t}$ respectively.

It turns out that (H, b) and $W_{s,t}$ are independent, the marginal distribution of H is Gaussian, and the marginal of b is logistic.

Proposition 3.2 (Distribution of Brownian bridge Lévy area [FLO20; Fos20]). *For fixed $0 \leq s < t < \infty$, the process $\{(H_{s,u}, b_{s,u})\}_{u \in [s,t]}$ and the increment $W_{s,t}$ are independent. Furthermore, H is distributed as a d-dimensional Gaussian with independent coordinates and the marginal distribution of each Brownian bridge Lévy area is logistic:*

$$H_{s,t} \sim \mathcal{N}^d \left(0, \frac{1}{12}(t-s) \right) \quad \text{and} \quad b_{s,t}^{(i,j)} \sim \text{Logistic} \left(0, \frac{1}{2\pi}(t-s) \right).$$

This yields the first two terms of the polynomial expansion of Lévy area.

6

Proposition 3.3 (Polynomial expansion of Lévy area [FH22])**.** *The Lévy area of a d-dimensional Brownian motion W has the following decomposition:*

$$A_{s,t} = H_{s,t} \otimes W_{s,t} - W_{s,t} \otimes H_{s,t} + b_{s,t},$$

where $\otimes$ denotes the outer-product of vectors.

This decomposition reduces the conditional generative task to the estimation of the Brownian bridge Lévy area conditional on the Brownian increment, where the target distribution and conditioning variable are independent. This approach may be generalised to the estimation of the tail sum of the polynomial expansion of Lévy area truncated at a higher level. Since B and the increment $W_{0,1} = w$ are independent, the conditional distribution $(B_t \mid W_{0,1} = w)$ is symmetric around 0. Furthermore, each dimension of B is its own independent process, so we can flip each individually without affecting the distribution, as established in the following lemma.

Lemma 3.4. *Let W be a d-dimensional Brownian motion on $[0,1]$ and let B, H, b be the corresponding derived processes from Definition 3.1. Fix some $\xi \in \{-1,1\}^d$, and let H', and b' be the space-time and space-space Lévy area processes associated with the process $\xi \odot B = \{\xi \odot B_t\}_{t \in [0,t]}$, where $\odot$ denotes the Hadamard (coordinate-wise) product. Then*

$$\{B_t\}_{t \in [0,1]} \overset{d}{=} \{\xi \odot B_t\}_{t \in [0,1]}, \quad H' = \xi \odot H, \quad b' = (\xi \otimes \xi) \odot b, \quad and \quad (H', b') \overset{d}{=} (H, b).$$

We also include a multiplication of a final independent random variable $\xi_0 \sim \mathrm{Rad}(\frac{1}{2})$, whose role is explained in Proposition C.3. Combining this with Lemma 3.4 we obtain the "bridge-flipping" function.

Definition 3.5. Let $w, h, \xi \in \mathbb{R}^d$, $b \in \mathbb{R}^{d \times d}$ and $\xi_0 \in \mathbb{R}$. Then the Bridge-flipping function is defined as

$$\mathrm{BF}(w, h, b, \xi_0, \xi) := \xi_0 \left((\xi \odot h) \otimes w - w \otimes (\xi \odot h) + (\xi \otimes \xi) \odot b \right), \tag{4}$$

for which we have the following as a consequence of Proposition 3.3, Lemma 3.4.

Theorem 3.6 (Bridge-flipping)**.** *Let $\xi_0, \dots, \xi_d \overset{i.i.d.}{\sim} \mathrm{Rad}(\frac{1}{2})$ be random variables so that W, (H, b), and $(\xi_0, \dots, \xi_d)$ are independent. Write $\xi = (\xi_1, \dots, \xi_d)$ and fix some $w \in \mathbb{R}^d$. Let H, b be as in Definition 3.1. Then for every $t \in [0,1]$*

$$\left(A_{0,t} \mid W_{0,1} = w \right) \overset{d}{=} \left(\mathrm{BF}\left(W_{0,t}, H_{0,t}, b_{0,t}, \xi_0, \xi \right) \mid W_{0,1} = w \right).$$

For our purpose, we will utilise the result for $t = 1$:

$$\left(A_{0,1} \mid W_{0,1} = w \right) \overset{d}{=} \mathrm{BF}\left(w, H_{0,1}, b_{0,1}, \xi_0, \xi \right).$$

Recall that $H_{s,t} \sim \mathcal{N}^d\left(0, \frac{1}{12}(t-s)\right)$, and that b and H are correlated, but that (H, b) and $W_{0,1}$ are independent. Hence, given a neural net $\mathrm{NN}_\theta : \mathbb{R}^{d+n} \to \mathbb{R}^d$, we define the "Bridge-flipping generation":

Algorithm 1 Area generation using Bridge-flipping

Input: θ - neural net parameters, d - Brownian dimension, w - Brownian increment, n - dimension of noise vector

1: $\xi_0 \leftarrow \mathrm{Rad}(1/2)$; $\xi \leftarrow \mathrm{Rad}^d(1/2)$
2: $h \leftarrow \mathcal{N}^d\left(0, \frac{1}{12}(t-s)\right)$; $z \leftarrow \mathcal{N}^n(0,1)$
3: $\widetilde{b} \leftarrow \mathrm{NN}_\theta(h, z)$ $\triangleright$ we want $\mathrm{NN}_\theta(h, z) \overset{d}{\approx} (b_{0,1} \mid H_1 = h)$
4: **return** $\mathrm{BF}\left(w, h, \widetilde{b}, \xi_0, \xi \right)$

This construction has some desirable properties.

1) Informally speaking, the use of ξ effectively makes the generator behave identically on all orthants of $\mathbb{R}^d$, and hence any learning done in one orthant transfers equally to the other orthants. This speeds up training and significantly improves the generator's accuracy, as it now perfectly mimics the symmetric structure of Lévy area.

2) The neural net can be trained directly on the distribution of $\left(b_{0,1} \mid H_{0,1} = h\right)$, and is then used for generation of $(A_{0,1}|W_{0,1} = w)$ using the BF algorithm.

3) The structure of BF allows for efficient implementation of back-propagation.

The use of the extra Rademacher random variable ξ_0 is to guarantee that all odd joint and conditional moments are correctly matched. This is summarised in Proposition C.3. Having $\widetilde{A}$ unbiased means that some of the usual error analysis from stochastic numerics can be applied, such as in the proof of Theorem 4.5, where one of the requirements is that $\widetilde{A}$ be unbiased. Recall that the Milstein scheme requires a subroutine which generates samples of Lévy area given a Brownian increment. Since $\widetilde{A} \sim \mathbb{P}_{\text{BF}}^{\theta,w}$ is unbiased, one can establish theoretical guarantees on the convergence of Milstein's method with the BF generator as this subroutine. The following result can be proven by applying [MT04, Theorem 1.1] with $p_1 = \frac{3}{2}$, $p_2 = 1$.

Proposition 3.7. *Given a time horizon $T > 0$, and a step size $h = \frac{T}{N}$ where $N \geq 1$ is the number of steps, let $\{\widetilde{X}_n\}_{n \in \{0, \cdots, N\}}$ be the output of Milstein's scheme (see Section G.2.1 for the definition) applied to the SDE*

$$dX_t = \mu(X_t, t)\,dt + \sigma(X_t, t)\,dW_t.$$

where the Lévy areas provided as input to Milstein's scheme were generated by the BF generator. Then if μ, σ are continuous and globally Lipschitz, there exists a constant $C > 0$ such that for sufficiently small h

$$\sup_{0 \leq n \leq N} \mathbb{E}\left[\left|\widetilde{X}_n - X_{nh}\right|^2\right]^{\frac{1}{2}} \leq Ch^{\frac{1}{2}}.$$

Remark 3.8. Although Theorem 3.6 and Algorithm 1 leads to the generation of $(A_{0,1}|W_{0,1} = w)$, we emphasize that it can be generalized to the generation of $(A_{0,t}|W_{0,1} = w)$ for any $t \in [0, 1]$ by using the scaling property of Brownian motion and its Lévy area. In particular, given w we can:

1) sample w' from the distribution of $\left(W_t|W_1 = w\right)$, i.e. $w' \sim \mathcal{N}\left(t\,w,\ t(1-t)\right)$.

2) rescale $w'' = \frac{w'}{\sqrt{t}}$ and sample $a'' \sim \left(A_{0,1} \mid W_1 = w''\right)$.

3) finally rescale again $a' = t\,a''$ which has the desired distribution $a' \sim \left(A_{0,t} \mid W_1 = w\right)$.

3.2 The Pair-net Generator

It is clear that for any $1 \leq i, j \leq d$, both $b_1^{(i,j)}$ and $A_1^{(i,j)}$ depend only on the paths of $\{W_t^{(i)}\}_{t \in [0,1]}$ and $\{W_t^{(j)}\}_{t \in [0,1]}$, but not on $\{W_t^{(k)}\}_{t \in [0,1]}$ for $k \notin \{i, j\}$. This dependency structure can be well described using graphs, encouraging us to employ model architectures reminiscent of Graph Neural Networks (GNN) [Sca+09].

Consider a clique on d nodes, where each node corresponds to one dimension of the Brownian motion, and each edge (i, j) is associated to $A^{(i,j)}$ (or $b^{(i,j)}$). Unlike GNNs, where it might be desirable for information to propagate throughout the entire graph, we want edge (i, j) to never see information at node $k \notin \{i, j\}$. Hence, our architecture should function like a 1-step GNN with edge-wise outputs.

So that $A^{(i,j)}$ only depends on $W^{(i)}$ and $W^{(j)}$, we generate a separate noise vector for each dimension of Brownian motion. We can interpret this as some embedding of the entire path $\{W_t^{(i)}\}_{t \in [0,1]} \mapsto$ noise$^{(i)}$, but in practice we use Gaussian noise.

Definition 3.9 (Pair-net). The Pair-net is defined as the mapping:

$$\text{PairNN}_\theta : (\mathbb{R}, \mathcal{Z}) \times (\mathbb{R}, \mathcal{Z}) \to \mathbb{R}; \quad (H, Z) \times (H', Z') \mapsto \widetilde{\mathbf{b}},$$

where $\mathcal{Z}$ be the space of latent noise. Consider $H_{0,1}$ and $b_{0,1}$ from Definition 3.1. We approximate $\mathbb{P}_{b_{0,1}|H_{0,1}=h}$ via

$$\widetilde{\mathbf{b}}^{(i,j)} = \text{PairNN}_\theta((h^{(i)}, \mathbf{z}^{(i)}), (h^{(j)}, \mathbf{z}^{(j)})), \quad 1 \leq i < j \leq d$$

for any $\mathbf{z} \in \mathcal{Z}^d$. In practice, we choose $\mathcal{Z}$ to be $\mathbb{R}^n$ and we let $\mathbf{z}^{(i)}$ be a n-dimensional Gaussian noise for $1 \leq i \leq d$. Combining this with bridge-flipping, we describe the generation algorithm and flowchart in Algorithm 2 and Figure 3.

Algorithm 2 Area generation using Pair-net generator and Bridge-flipping
---
Input: θ - neural net parameters, d - dimension of Brownian motion, w - Brownian increment, n - dimension of noise vector associated with each coordinate of Brownian motion.

1: $\xi_0 \leftarrow \mathrm{Rad}(1/2) ; \quad \xi \leftarrow \mathrm{Rad}^d(1/2)$
2: $\mathbf{z}^{(i)} \leftarrow \mathcal{N}^n(0,1)$ for $1 \leq i \leq d; \quad h \leftarrow \mathcal{N}^d\big(0, \frac{1}{12}(t-s)\big)$
3: $\widetilde{b}^{(i,j)} \leftarrow \mathrm{PairNN}_\theta\big((h^{(i)}, \mathbf{z}^{(i)}), (h^{(j)}, \mathbf{z}^{(j)})\big)$ for $1 \leq i < j \leq d$
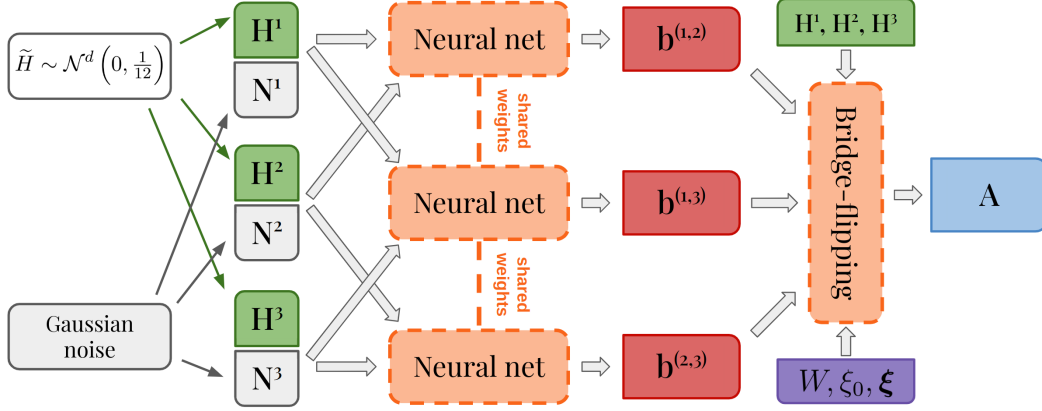4: **return** $\mathrm{BF}\big(w, h, \widetilde{b}, \xi_0, \xi\big)$

Figure 3: A schematic of the Pair-net architecture when $d = 3$.

This solves the issue of permutation equivariance, but there is another requirement to be enforced: $b^{(i,j)} = -b^{(j,i)}$. Hence we want

$$\mathrm{PairNN}_\theta\Big(h^{(i)}\|\mathbf{z}^{(i)}\|h^{(j)}\|\mathbf{z}^{(j)}\Big) = -\mathrm{PairNN}_\theta\Big(h^{(j)}\|\mathbf{z}^{(j)}\|h^{(i)}\|\mathbf{z}^{(i)}\Big).$$

It is possible to build this into the architecture itself, but that comes at the cost of doubling the computation time, and results in a bimodal output distribution, which is undesirable. Instead, we add an "anti-symmetric-penalty" to the generator loss, controlled by the hyperparameter λ_{ASP}:

$$L_{\mathrm{ASP}} := \lambda_{\mathrm{ASP}} \, \mathbb{E}_{\mathbf{z},\mathbf{h}} \left[\sum_{1 \leq i < j \leq d} \left(\mathrm{PairNN}_\theta\Big(h^{(i)}\|\mathbf{z}^{(i)}\|h^{(j)}\|\mathbf{z}^{(j)}\Big) + \mathrm{PairNN}_\theta\Big(h^{(j)}\|\mathbf{z}^{(j)}\|h^{(i)}\|\mathbf{z}^{(i)}\Big) \right)^2 \right].$$

Indeed, it can be seen empirically that this new formulation leads to substantially better permutation invariance. The simplest way to test this is to fix some $\mathbf{h} \in \mathbb{R}^4$ and let $\mathbf{h}'$ be equal to $\mathbf{h}$ with the first two dimensions swapped. We then generate two batches of bridge Lévy areas $\widetilde{\mathbf{b}}$ and $\widetilde{\mathbf{b}}'$ conditional on $\mathbf{h}$ and $\mathbf{h}'$ respectively. Finally, we can permute the dimensions of $\widetilde{\mathbf{b}}'$ in the appropriate way, i.e.

$$\widetilde{\mathbf{b}}'^{(1,2)} \leftarrow -\widetilde{\mathbf{b}}'^{(1,2)} \qquad \widetilde{\mathbf{b}}'^{(1,3)} \longleftrightarrow \widetilde{\mathbf{b}}'^{(2,3)} \qquad \widetilde{\mathbf{b}}'^{(2,4)} \longleftrightarrow \widetilde{\mathbf{b}}'^{(1,4)}. \tag{5}$$

If the generator is permutation invariant, then this should yield $\widetilde{\mathbf{b}} \overset{d}{\approx} \widetilde{\mathbf{b}}'$. Figure 4 shows the results of such a comparison for a) a somewhat-trained Pair-net generator, and b) a slightly better trained BF generator.

Another benefit of the Pair-net architecture is that the neural net PairNN_θ can now be significantly smaller since it does not need to capture the relationship between all the dimensions. This comes with the downside of requiring more passes through it (as shown in Figure 3, we use a single net to generate all b's, each dimension of b requires its own forward pass), but suitable indexing and batching can make this efficient. Indeed, using PairNet results in both a speed-up and greater accuracy (see Section 6).

Furthermore, we emphasize that the PairNet structure allows us to generate Lévy area for any dimension d', even though we train the model in a lower dimension $d < d'$. From now on, we will take nsz to be the total noise dimension for the complete Lévy area generation, namely, $\mathrm{nsz} = n \times d$
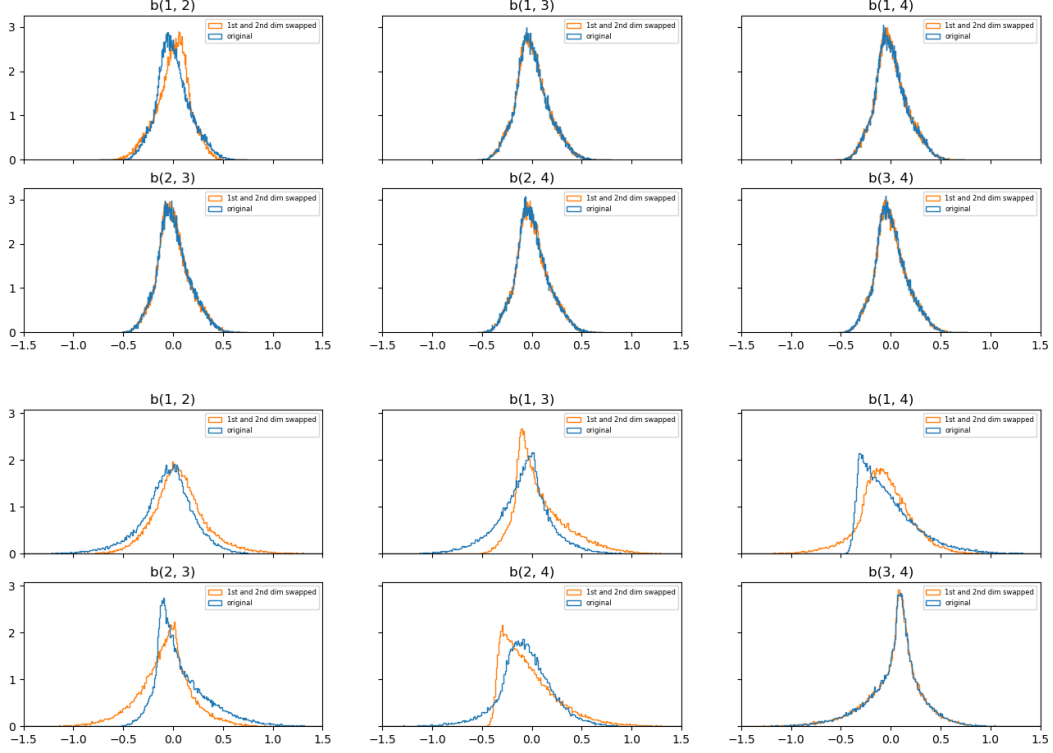
Figure 4: Probability densities estimated using samples from the generator with the first two input dimensions swapped (orange) and without swapping (blue) for Pair-net (top), and the BF generator (bottom). The blue and orange plots should overlap as best as possible.

where n is the latent noise dimension and d denotes the Brownian dimension. In the framework of Definition 2.1, our generator is now $G_\theta : \mathbb{R}^d \times \mathbb{R}^{\mathrm{nsz}} \to \mathbb{R}^d \times \mathbb{R}^a$ and the evaluation follows Algorithm 2.

4 Discriminator

One potential discriminator is the characteristic function GAN (CFGAN) approach introduced in [FSS20; Li+20a], which aims to learn the law of an underlying process by approximating its characteristic function. Compared to traditional GANs, we list some advantages of this approach:

1) The characteristic function always exists and is uniformly bounded.

2) The characteristic function fully describes the law of the random variable, hence offering good theoretical support.

In this section, we introduce two different choices for the characteristic function. Firstly, we assess the distance between two distributions using the characteristic function distance.

Definition 4.1 (Characteristic function distance [FSS20]). Let $\mathbb{P}_X$ and $\mathbb{P}_Y$ be the distributions of two $\mathbb{R}^d$-valued random variable X and Y respectively. The characteristic function distance (CFD) between X and Y associated with an $\mathbb{R}^d$-valued random variable $\Lambda \sim \nu$ is given by

$$\mathrm{CFD}_\Lambda(X, Y) = \mathbb{E}_{\Lambda \sim \nu}\left[\left\|\Phi_X(\Lambda) - \Phi_Y(\Lambda)\right\|\right],$$

where $\Phi_X(\Lambda) := \mathbb{E}_{X \sim \mathbb{P}_X}[\exp i\langle \Lambda, X\rangle]$.

The characteristic function distance has the following properties:

1) Definiteness: If the support of Λ is $\mathbb{R}^d$, then $\mathrm{CFD}_\Lambda(X, Y) = 0$ iff $\mathbb{P}_X = \mathbb{P}_Y$.

2) The distance is bounded and differentiable almost everywhere.

3) For certain ν, $\mathrm{CFD}_\Lambda(X, Y_n) \to 0 \implies Y_n \xrightarrow{d} X$ ([Sri+10],Proposition A.2).

If we restrict ν to be a member of the family of certain well-known distributions, Gaussian for example, we can parameterize the distribution ν by learnable coefficients and it will play the role of discriminator in the GAN setting. The backpropagation on these coefficients is well-understood by techniques such as the reparameterization trick. In practice, we approximate the characteristic function by an empirical measure: if $\Lambda \sim \nu$, and $x_1, \ldots, x_N$ are samples from $\mathbb{P}_X$, then we estimate $\Phi_X(\Lambda)$ by

$$\widehat{\Phi}_X(\Lambda) = \frac{1}{N} \sum_{i=1}^{N} \exp\left(i \langle \Lambda, x_i \rangle\right).$$

The use of the empirical characteristic function in place of the analytical characteristic function is justified in Proposition A.1. However, if $X = (W_t, A_t)$, i.e. the joint process of d-dimensional Brownian motion and the corresponding Lévy area at any time t, we may obtain $\Phi_{(W_t, A_t)}$ analytically, see Theorem C.1.

4.1 Unitary characteristic function

In this subsection, we introduce an extension of the classical characteristic function of a random variable, originally proposed in [CL16] and [LLN23]. We denote by U_n the set of unitary matrices of dimension n, then U_n is a matrix Lie group with the group operation of matrix multiplication. The Lie algebra of U_n, denoted by $\mathfrak{g}_n$ is the set of anti-hermitian matrices, i.e. $\mathfrak{g}_n := \{A \in \mathbb{C}^{n \times n} : A^* + A = 0\}$. Next, we give a definition of the unitary representation of a random variable and its unitary characteristic function.

Definition 4.2 (Unitary characteristic function). Let $X \sim \mathbb{P}_X$ be a $\mathbb{R}^d$-valued random variable. Let $n \geq 1$ be an integer. Denote by U_n and $\mathfrak{g}_n$ the unitary matrix Lie group of degree n and its corresponding Lie algebra. Let $M \in \mathcal{L}(\mathbb{R}^d, \mathfrak{g}_n)$, the *unitary representation function* of X is given by the mapping :
$$\mathcal{U}_M(X) := \exp(M(X)) \tag{6}$$
where $\exp$ denotes the matrix exponential. The *unitary characteristic function* of X is defined as a mapping from $L(\mathbb{R}^d, \mathfrak{g}_n)$ to $GL(n)$ such that
$$\mathrm{UCF}_n(X)(M) := \mathbb{E}_{X \sim \mathbb{P}_X}[\mathcal{U}_M(X)] \tag{7}$$
In practice, $\mathrm{UCF}_n(X)(M)$ is approximated by Monte-Carlo. Let $\mathbf{X} = \{X_i\}_{i=1}^{N}$ be N samples from $\mathbb{P}_X$. The *empirical unitary characteristic function* is given by

$$\mathrm{EUCF}_n(\mathbf{X})(M) := \frac{1}{N} \sum_{i=1}^{N} \mathcal{U}_M(X_i).$$

Remark 4.3. If $n = 1$, then $\mathfrak{g}_1$ is just the set of pure imaginary numbers and M can be identified with an element $\lambda \in \mathbb{R}^d$ such that $M(x) = i\langle \lambda, x \rangle$ for all $x \in \mathbb{R}^d$ where $\langle \cdot, \cdot \rangle$ denotes the standard inner product. Then, $\mathrm{UCF}_1(X)$ recovers the standard characteristic function of a d-dimensional random variable.

Similar to Definition 4.1, for any $n \geq 1$, we can define the *unitary characteristic function distance* for two random variables X and Y as

$$\mathrm{UCFD}_n^2(X, Y) = \mathbb{E}_{M \sim \mathbb{P}_\mathcal{M}}\left[\left\|\mathrm{UCF}_n(X)(M) - \mathrm{UCF}_n(Y)(M)\right\|_{HS}^2\right].$$

where $\mathbb{P}_\mathcal{M}$ denotes the distribution of the linear mapping M and $\|\cdot\|_{HS}$ denotes the Hilbert–Schmidt norm. As was the case with the discriminator for the standard characteristic function, we parameterize the law of linear mappings $\mathbb{P}_\mathcal{M}$ by an empirical measure

$$\mathbb{P}_\mathcal{M} = \frac{1}{N} \sum_{i=1}^{N} \delta_{M_i},$$

where δ denotes the Dirac measure and each M_i can be parametrized as learnable coefficients and optimized using gradient-based methods. For computation and optimization details of UCFD, please refer to [LLN23]. Let $X = (W_1, A_1)$, then the benefits of UCFD compared to the standard characteristic function distance include:

1) Standard uniqueness results hold as $\text{UCF}_1(X)$ recovers the standard characteristic function.

2) Since $\mathfrak{g}_1$ is a subspace of $\mathfrak{g}_n$ for any $n > 2$, $\mathcal{U}_M$ possesses a richer structure than $\mathbb{C}$ for any linear mapping M into $\mathfrak{g}_n$. Although using $\mathfrak{g}_1$ already encodes enough information to determine the random variable, embedding the random variable into Lie algebra of a higher degree appears to provide a more efficient way of representing the information that characterizes the random variable. Empirically, using the unitary characteristic function led to a more stable training procedure compared to the standard one.

4.2 Chen Training

While Brownian motion over different intervals can be concatenated simply via addition, i.e. $W_{0,t} = W_{0,s} + W_{s,t}$, concatenation of Lévy areas requires an additional term, specified by Chen's relation. In its general version within rough path theory, Chen's relation establishes the homomorphism property of path signatures under concatenation [LCL07, Theorem 2.9]. However, we will present just the special case relating to Lévy area.

Proposition 4.4 (Chen's relation [Che57]). *For times $0 < s < t$*

$$A_{0,t}^{(i,j)} = A_{0,s}^{(i,j)} + A_{s,t}^{(i,j)} + \frac{1}{2}\left(W_{0,s}^{(i)}W_{s,t}^{(j)} - W_{0,s}^{(j)}W_{s,t}^{(i)}\right).$$

We now present the main theoretical contribution of this section, which can be viewed as a partial converse of the above proposition.

Theorem 4.5. *[Distributional uniqueness of Lévy area under Chen's relation]*

Suppose μ is a mean zero probability distribution on $\mathbb{R}^d \times \mathbb{R}^{d \times d}$, where the first marginal has finite second moment. Let $(V_i, Z_i) \overset{i.i.d.}{\sim} \mu$ for $i = 1, 2$; if it holds that

$$V_3 := \frac{1}{\sqrt{2}}\left(V_1 + V_2\right), \quad Z_3 := \frac{1}{2}Z_1 + \frac{1}{2}Z_2 + \frac{1}{4}\left(V_1 \otimes V_2 - V_2 \otimes V_1\right) \tag{8}$$

is also distributed according to μ, then μ is the distribution of $(W_{0,1}, A_{0,1})$ where A is the Lévy area process associated with a d-dimensional Brownian motion W.

Including a finite-variance assumption on the measure μ, and a Gaussian assumption on the first marginal, provides an alternative proof using Wasserstein distances (see Theorem B.3). The preceding motivates the following procedure, which takes samples Z_1, Z_2 from some distribution and concatenates them using Chen's relation to produce samples that are closer in distribution to $A_{0,1}$. With abuse of notation, if $\mathbf{X} \in \mathbb{R}^{m \times d}$ consists of m samples of a d-dimensional random variable, we denote by $\mathbf{X}^{(i)} \in \mathbb{R}^m$ the i-th coordinate of each sample. Adopting this notation, we describe the Chen-combine operation in Algorithm 3.

We also note that the proof of Theorem B.3 shows that the repeated application of Chen-combine gives convergence of order at least $\frac{1}{2}$ in the 2-Wasserstein metric. Faster rates can be proven assuming a suitable starting distribution, such as Davie's approximation [Dav14; FL15].

Remark 4.6. Let $\widetilde{\mathbf{A}}$ be the estimated Lévy area given a fixed Brownian increment $\mathbf{W}$. Let $\widetilde{\mathbf{A}}_{\text{Chen}}$ be the resulting Lévy area process of $\text{Chen-combine}(\mathbf{W}, \widetilde{\mathbf{A}})$. In Theorem B.4 we show that (informally speaking)

$$\mathcal{W}_2\left(\widetilde{\mathbf{A}}, \mathbf{A}_{\text{true}}\right) \leq \left(2 + \sqrt{2}\right)\mathcal{W}_2\left(\widetilde{\mathbf{A}}, \widetilde{\mathbf{A}}_{\text{Chen}}\right),$$

where $\mathcal{W}_2$ denotes the $2-$Wasserstein metric. So, in order to minimise $\mathcal{W}_2(\widetilde{\mathbf{A}}, \mathbf{A}_{\text{true}})$, we need only minimise $\mathcal{W}_2(\widetilde{\mathbf{A}}, \widetilde{\mathbf{A}}_{\text{Chen}})$, which requires no "true" samples of Lévy area to compute. This allows us to modify the training objective of the GAN so that it will learn the correct distribution *without any access to externally supplied data*.

Assume $(\mathbf{W}, \widetilde{\mathbf{A}}) \in \mathbb{R}^{2m \times (d+a)}$ is $2m$ samples of $(d+a)$-dimensional random variable. By Chen-combine$(\mathbf{W}, \widetilde{\mathbf{A}})$ we mean: evenly split $(\mathbf{W}, \widetilde{\mathbf{A}})$ into two blocks with equal size, denoted by $(\mathbf{W}, \widetilde{\mathbf{A}})_{\text{first}}, (\mathbf{W}, \widetilde{\mathbf{A}})_{\text{second}} \in \mathbb{R}^{m \times (d+a)}$, and apply the operation described in Algorithm 3. The output of Chen-combine will be an element in $\mathbb{R}^{m \times (d+a)}$.

Algorithm 3 Chen-combine

Input: m - batch size, d- Brownian dimension, a- Lévy dimension, $(\mathbf{W}, \widetilde{\mathbf{A}})_{\text{first}} \in \mathbb{R}^{m \times (d+a)}$, $(\mathbf{W}, \widetilde{\mathbf{A}})_{\text{second}} \in \mathbb{R}^{m \times (d+a)}$ - Brownian increments and Lévy area samples.

1: $\widehat{\mathbf{W}} \leftarrow \mathbf{0} \in \mathbb{R}^{m \times d}, \widehat{\mathbf{A}} \leftarrow \mathbf{0} \in \mathbb{R}^{m \times a}$

2: $\mathbf{W}_{\text{first}} \leftarrow \frac{1}{\sqrt{2}} \mathbf{W}_{\text{first}}, \mathbf{W}_{\text{second}} \leftarrow \frac{1}{\sqrt{2}} \mathbf{W}_{\text{second}},$ ▷ Brownian scaling $W_{0,\frac{1}{2}} \overset{d}{=} \frac{1}{\sqrt{2}} W_{0,1}$

3: $\widetilde{\mathbf{A}}_{\text{first}} \leftarrow \frac{1}{2} \widetilde{\mathbf{A}}_{\text{first}}, \widetilde{\mathbf{A}}_{\text{second}} \leftarrow \frac{1}{2} \widetilde{\mathbf{A}}_{\text{second}},$ ▷ Brownian scaling $A_{0,\frac{1}{2}} \overset{d}{=} \frac{1}{2} A_{0,1}$

4: **for** $i \in \{1, \ldots, d\}$ **do**

5:   $\widehat{\mathbf{W}}^{(i)} \leftarrow \mathbf{W}_{\text{first}}^{(i)} + \mathbf{W}_{\text{second}}^{(i)}$

6:   **for** $j \in \{i+1, \ldots, d\}$ **do**

7:     $\mathbf{D} \leftarrow \frac{1}{2} \left(\mathbf{W}_{\text{first}}^{(i)} \odot \mathbf{W}_{\text{second}}^{(j)} - \mathbf{W}_{\text{first}}^{(j)} \odot \mathbf{W}_{\text{second}}^{(i)} \right)$

8:     $\widehat{\mathbf{A}}^{(i,j)} \leftarrow \widetilde{\mathbf{A}}_{\text{first}}^{(i,j)} + \widetilde{\mathbf{A}}_{\text{second}}^{(i,j)} + \mathbf{D},$ ▷ Chen's relation

9: **return** $(\widehat{\mathbf{W}}, \widehat{\mathbf{A}})$

---

5   LévyGAN

In this section, we incorporate the ideas presented in Sections 3 and 4 into our tailored model, named LévyGAN used to generate the associated Lévy area conditioned on the Brownian increments. Similar to Definition 2.1, we provide the definition of the proposed model as follows.

Definition 5.1 (LévyGAN)**.** Let PairNN$_\theta$ denote a PairNet generator defined in Definition 3.9. Given a d-dimensional Brownian increment at $t = 1$, $W \sim \mathcal{N}^d(0, 1)$, for all $1 \le i < j \le d$, we generate estimated Lévy area associated to W as follows:

$$\widetilde{b}^{(i,j)} = \text{PairNN}_\theta((H^{(i)}, Z^{(i)}), (H^{(j)}, Z^{(j)})) \tag{9}$$

$$\widetilde{A}^{(i,j)} = H^{(i)} W^{(j)} - H^{(j)} W^{(i)} + \widetilde{b}^{(i,j)} \tag{10}$$

Let $\mathbf{w} \in \mathbb{R}^{N \times d}$ be N samples of Brownian increment and the associated $\widetilde{\mathbf{A}} \in \mathbb{R}^{N \times a}$ generated according to Equations (9) and (10), then we construct new samples using Chen-combine defined in Algorithm 3:

$$(\mathbf{w}_{\text{Chen}}, \widetilde{\mathbf{A}}_{\text{Chen}}) \coloneqq \text{Chen-combine}(\mathbf{w}, \widetilde{\mathbf{A}}).$$

For $m \ge 1$, let $\mathfrak{g}_m$ be the Lie algebra of the unitary matrix group U_m. Recall EUCF$_m$ from in Definition 4.2, and let $\mathcal{M} = \{M_i\}_{i=1}^M$, $M_i \in L(\mathbb{R}^{d+a}, \mathfrak{g}_m)$ be a collection of linear mappings onto $\mathfrak{g}_m$, each of them parametrized by an element in $\mathbb{R}^{(d+a) \times \dim(\mathfrak{g}_m)}$. $\mathcal{M}$ will play the role of the discriminator. Finally, the training is performed with respect to the following min-max game

$$\min_\theta \max_\mathcal{M} \text{Loss}(\theta, \mathcal{M}; \mathbf{w}),$$

where $\text{Loss}(\theta, \mathcal{M}; \mathbf{w}) \coloneqq \text{EUCFD}_m\big((\mathbf{w}, \widetilde{\mathbf{A}}), (\mathbf{w}_{\text{Chen}}, \widetilde{\mathbf{A}}_{\text{Chen}})\big)$. The training algorithm and flowchart are described in Algorithm 4 and Figure 5.

Remark 5.2. One can interpret Chen training as a type of adaptive training, where the "almost true" target data $\widetilde{\mathbf{A}}_{\text{Chen}}$ is always just sufficiently better than the generator's output, that training can progress effectively. Thus, instead of requiring large datasets of "true" samples, which are costly to generate and difficult to handle, we can now very efficiently generate new "true" data on the fly, of any desired quantity and of just the right precision. One could choose to iteratively apply

13

Chen-combine several times, but we have observed that training is slightly faster and more efficient when only a single application of Chen combined is used in Algorithm 4. This is because using two Chen-combines produces twice fewer "true" samples and reducing the sample size leads to a poorer estimate of EUCFD.

Algorithm 4 Training algorithm for LévyGAN

Input: d - Brownian dimension, a - Lévy area dimension, n - noise dimension, m - Lie algebra degree, M - number of linear mappings onto $\mathfrak{g}_m$, PairNN$_\theta$ - generator, $\mathcal{M} \in \mathbb{R}^{M \times (d+a) \times \dim(\mathfrak{g}_m)}$ - discriminator, iter$_d$ - number of discriminator updates per generator update, bsz - batch size, η_g, η_d - generator and discriminator learning rates.

 1: **while** $\theta, \mathcal{M}$ not converge **do**
 2:     **for** $i \in (1, \ldots, \text{iter}_d)$ **do**
 3:         Sample $\mathbf{w} \sim \mathcal{N}^d(0,1)$, $(\mathbf{h}, \mathbf{z}) \sim \mathcal{N}^d(0, \frac{1}{12}) \times \mathcal{N}^{d \times n}(0,1)$ of size $2\,\mathtt{bsz}$.
 4:         $\widetilde{\mathbf{b}}^{(i,j)} \leftarrow \text{PairNN}_\theta((\mathbf{h}^{(i)}, \mathbf{z}^{(i)}), (\mathbf{h}^{(j)}, \mathbf{z}^{(j)}))$ for $1 \leq i < j \leq d$
 5:         $\xi_0 \leftarrow \text{Rad}(1/2)$, $\boldsymbol{\xi} \leftarrow \text{Rad}^d(1/2)$
 6:         $\widetilde{\mathbf{A}} \leftarrow \text{BF}(\mathbf{w}, \mathbf{h}, \widetilde{\mathbf{b}}, \xi_0, \boldsymbol{\xi})$
 7:         $\mathbf{w}_{\text{Chen}}, \widetilde{\mathbf{A}}_{\text{Chen}} \leftarrow \text{Chen-combine}(\mathbf{w}, \widetilde{\mathbf{A}})$
 8:         $\text{Loss}(\theta, \mathcal{M}; \mathbf{w}) \leftarrow \text{EUCFD}_m((\mathbf{w}, \widetilde{\mathbf{A}}), (\mathbf{w}_{\text{Chen}}, \widetilde{\mathbf{A}}_{\text{Chen}}))$
 9:         $\mathcal{M} \leftarrow \mathcal{M} - \eta_d \cdot \nabla_{\mathcal{M}}(-\text{Loss}(\theta, \mathcal{M}; \mathbf{w}))$ ▷ Maximize the loss
10:     Sample $\mathbf{w} \sim \mathcal{N}^d(0,1)$, $(\mathbf{h}, \mathbf{z}) \sim \mathcal{N}^d(0, \frac{1}{12}) \times \mathcal{N}^{d \times n}(0,1)$ of size $2\,\mathtt{bsz}$.
11:     $\widetilde{\mathbf{b}}^{(i,j)} \leftarrow \text{PairNN}_\theta((\mathbf{h}^{(i)}, \mathbf{z}^{(i)}), (\mathbf{h}^{(j)}, \mathbf{z}^{(j)}))$ for $1 \leq i < j \leq d$
12:     $\xi_0 \leftarrow \text{Rad}(1/2)$, $\boldsymbol{\xi} \leftarrow \text{Rad}^d(1/2)$
13:     $\widetilde{\mathbf{A}} \leftarrow \text{BF}(\mathbf{w}, \mathbf{h}, \widetilde{\mathbf{b}}, \xi_0, \boldsymbol{\xi})$
14:     $\mathbf{w}_{\text{Chen}}, \widetilde{\mathbf{A}}_{\text{Chen}} \leftarrow \text{Chen-combine}(\mathbf{w}, \widetilde{\mathbf{A}})$
15:     $\text{Loss}(\theta, \mathcal{M}; \mathbf{w}) \leftarrow \text{EUCFD}_m((\mathbf{w}, \widetilde{\mathbf{A}}), (\mathbf{w}_{\text{Chen}}, \widetilde{\mathbf{A}}_{\text{Chen}}))$
16:     $\theta \leftarrow \theta - \eta_d \cdot \nabla_\theta \text{Loss}(\theta, \mathcal{M}; \mathbf{w})$ ▷ Minimize the loss
17: **return** PairNN$_\theta, \mathcal{M}$

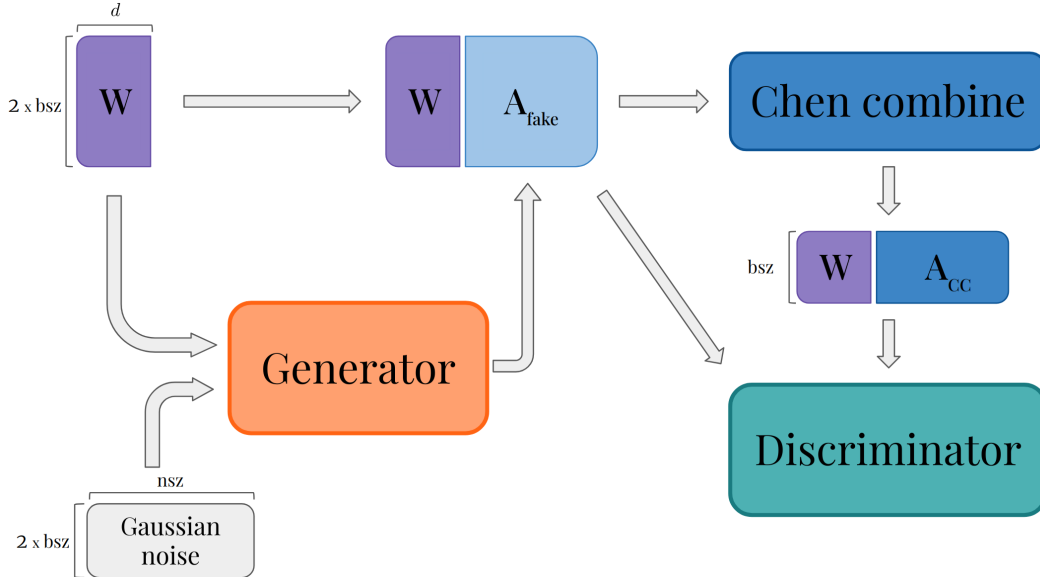

Figure 5: A schematic of LévyGAN. Here bsz denotes the batch dimension and we recall that nsz denotes the total noise dimension, namely $nsz = n \times d$.

14

6 Numerical Experiments

We train the model in $d = 4$. Note that by the architecture of the generator, the model can be used to generate Brownian Lévy area for any $d' \leq d$. The model can be also used to generate Lévy area for any $d' > d$, however, the performance might be deteriorated as training is not done for higher dimensions.

We performed the training procedure as illustrated in Algorithm 4. On the generator side, we used a Feed-forward Neural Network. The activation function is chosen to be LeakyRelu function. On the discriminator side, we parameterize 128 linear maps onto the Lie algebra of degree 3 to mimic the empirical distribution used to compute UCFD mentioned in Section 4.1. The total number of training iterations is set to be 2500, where we observed the convergence on the marginal 2-Wasserstein metric on real data. We optimize both the generator and discriminator using Stochastic Gradient Descent and Adam optimizer. We set the batch size to 2^{13} and the learning rate for generator/discriminator is set to be 0.001/0.01 respectively. Both learning rates decay for each 500 iteration. Finally, we set iter_d to be 3.

We conducted a hyperparameter grid-search (see Section E), evaluating the model performance according to the marginal 2-Wasserstein metric, with our optimal architecture as follows:

- Feed-forward Neural Network with 3 hidden layers and 16 hidden dimensions.

- LeakyRelu activation function with slope $= 0.01$.

- Gaussian noise with $n = 3$.

Finally, we assess the performance of our model on the generation of the coupled process for $d = 2,\ 3,\ 4$, and 8. We consider the following test metrics:

1) Marginal 2-Wasserstein metric.

2) Cross moment metric.

3) Characteristic Function Distance, using Maximum Mean Discrepancy with different kernels.

4) Empirical Unitary Characteristic Function.

A detailed explanation of each test metric can be found in Section D. We compare with two baselines: Foster's and Davie's moment matching generator [Fos20; Fos25; Dav14], and we regard the truncated Fourier series [KR23] of Lévy area up to an L^2 precision of 10^{-4} as "true" samples. Finally, we provide a numerical example for the log-Heston model using different estimators for fake Lévy area.

Test Metric	LévyGAN	Foster	Davie	Fourier series
Computational time (s)	0.019	0.0071	0.002	3.1
Marginal W_2 (10^{-2})	$\mathbf{.246 \pm .013}$	$.254 \pm .010$	$2.03 \pm .013$	$.27 \pm 0.008$

Table 1: Marginal distribution fitting and computational efficiency for the different generative models. The generation is done using NVIDIA Quadro RTX 8000. The marginal W_2 error is calculated with respect to the joint process generated by the Fourier series. Tests are performed with 2^{20} samples. The final column contains the results of the Fourier algorithm with 19 terms in the expansion (far more terms were used to generate "true" samples). This truncation has been chosen so that the performance is comparable to LévyGAN and Foster's method.

Dim	Test Metrics	LévyGAN	Foster	Davie
	Fourth moment	$.004 \pm .002$	$\mathbf{.002 \pm .002}$	$.042 \pm .001$
2	Polynomial MMD (10^{-5})	$\mathbf{.341 \pm .070}$	$.654 \pm .131$	$.646 \pm .188$
	Gaussian MMD (10^{-6})	$1.47 \pm .125$	$\mathbf{1.44 \pm .128}$	$34.6 \pm .683$
	EUCFD (10^{-2})	$\mathbf{1.52 \pm .213}$	$1.92 \pm .113$	$10.1 \pm .851$
	Fourth moment	$\mathbf{.004 \pm .002}$	$\mathbf{.004 \pm .002}$	$.043 \pm .001$
3	Polynomial MMD (10^{-5})	$\mathbf{2.18 \pm .568}$	$2.30 \pm .732$	$2.26 \pm .773$
	Gaussian MMD (10^{-6})	$1.87 \pm .002$	$\mathbf{1.84 \pm .001}$	$16.3 \pm .001$
	EUCFD (10^{-2})	$\mathbf{1.88 \pm .063}$	$2.03 \pm .034$	18.5 ± 1.11
	Fourth moment	$\mathbf{.004 \pm .000}$	$.006 \pm .002$	$.043 \pm .002$
4	Polynomial MMD (10^{-5})	$\mathbf{4.04 \pm .436}$	4.65 ± 1.31	$5.62 \pm .808$
	Gaussian MMD (10^{-6})	$\mathbf{1.90 \pm .001}$	$\mathbf{1.90 \pm .001}$	$263 \pm .003$
	EUCFD (10^{-2})	$\mathbf{1.92 \pm .026}$	$2.03 \pm .036$	$17.5 \pm .483$
	Fourth moment	$.006 \pm .001$	$.006 \pm .002$	$.044 \pm .000$
8	Polynomial MMD (10^{-2})	$\mathbf{1.13 \pm .019}$	$1.15 \pm .030$	$1.31 \pm .066$
	Gaussian MMD (10^{-6})	$\mathbf{1.91 \pm .001}$	$\mathbf{1.91 \pm .000}$	$1.92 \pm .003$
	EUCFD (10^{-2})	$\mathbf{1.99 \pm .002}$	$\mathbf{1.99 \pm .001}$	$2.05 \pm .003$

Table 2: Fourth moment and MMD-based metrics across different models and Brownian dimensions.

6.1 SDE Example

In this section, we will demonstrate how "fake" Lévy area can be used within SDE numerics to achieve both high order weak convergence as well as Multilevel Monte Carlo (MLMC) variance reduction. Although the synthetic Lévy area only needs to exhibit the correct mean and covariance to give high order weak convergence, we show that the bias introduced by the MLMC estimator is negligible in practice due to the small Chen error inherent in our generative model. A secondary motivation is to compare the various Lévy area generators and show that our GAN-based approach performs indistinguishably from previous state-of-the-art methods – whilst taking less time to generate samples.

Consider the Itô SDE from Equation (1)

$$dX_t = f(X_t)dt + \sum_{i=1}^{d} g_i(X_t)dW_t^{(i)}, \quad X_0 = x_0, \tag{1 revisited}$$

where the solution X takes values in $\mathbb{R}^e$. To estimate the solution to Equation (1) one typically uses a discretisation scheme that generates approximate sample paths of the solution X. Often the objective is to approximate quantities of the form

$$\mathbb{E}\left[\varphi(X) \mid X_0 = x_0\right], \tag{11}$$

where φ may depend on the whole sample path $(X_t)_{t \in [0,T]}$, though commonly it is only a function of the solution X_T at the terminal time T. To measure the error of a particular discretisation scheme, there are two standard metrics: weak and strong error. We will only evaluate the weak error for reasons discussed in Section G.1. To accurately determine the error of various numerical schemes, we seek a multidimensional SDE and a quantity of the form (11) which is known semi-analytically. Thankfully, such an example exists: the price of a European call option under the log-Heston model. The stochastic volatility model is defined by the following two-dimensional SDE:

$$
\begin{aligned}
dU_t &= \left(r - \frac{1}{2}V_t\right)dt + \sqrt{V_t}\,dW_t^{(1)}, \quad U_0 \in \mathbb{R} \\
dV_t &= \kappa(\theta - V_t)dt + \sigma\sqrt{V_t}\,dW_t^{(2)}, \quad V_0 > 0,
\end{aligned}
\tag{12}
$$

for a pair of independent Brownian motions $W^{(1)}$ and $W^{(2)}$. To ensure the volatility term V remains positive, we must enforce the Feller condition $2\kappa\theta - \sigma^2 > 0$. The payoff of a European call option for a price process S with $S := \exp(U)$ is given by

$$\varphi(S) := e^{-rT}\left(e^{U_T} - K\right)^+,$$

where r is the discount rate, K the strike price, and T the maturity. For the derivation and form of the semi-analytic formula for the expected value of the above, we refer the reader to [Ter22] and [Cri15].

6.2 Numerical Results

We compare four discretisation schemes combined with multilevel Monte-Carlo (MLMC) [Gil08]. We briefly recall that MLMC is based on the idea of a telescoping sum of expectations. Indeed, assume we have L levels, and that Y_l is an estimator for X, based on a discretisation scheme with step-size h_l, then we may write

$$\mathbb{E}\left[\varphi\left(Y_L\right)\right] = \sum_{l=1}^{L} \mathbb{E}\left[\varphi\left(Y_l\right) - \varphi\left(Y_{l-1}\right)\right],$$

with $Y_0 \equiv 0$. The MLMC estimator is then defined by

$$\overline{\varphi}_{n_1,\dots,n_L} = \sum_{l=1}^{L} \widehat{\varphi}_{n_l}, \quad \text{where} \quad \widehat{\varphi}_{n_l} = \frac{1}{n_l}\sum_{i=1}^{n_l}\left(\varphi\left(Y_l^{i,l}\right) - \varphi\left(Y_{l-1}^{i,l}\right)\right), \tag{13}$$

where $Y_l^{i,l}$ is the ith sample of the estimator Y_l used on level l, and $Y_{l-1}^{i,l}$ is the ith sample of the estimator Y_{l-1} that is used on level l. It is important to note that the pairs $(Y_l^{i,l}, Y_{l-1}^{i,l})$ are coupled: the underlying Brownian path for each member of the pair is the same. In our case, the path on the lower level will be coarse (i.e. a large step size) and the higher level will be fine (i.e. a small step size). The standard condition used to ensure convergence of the telescoping sum of expectations is given by

$$\mathbb{E}\left[\varphi\left(Y_l^{\cdot,l}\right)\right] = \mathbb{E}\left[\varphi\left(Y_l^{\cdot,l+1}\right)\right].$$

However, when incorporating a fake Lévy area term, our coupling at each level is defined as follows.

1) The Brownian increments for the fine path $Y_l^{\cdot,l}$ are generated with step size h_l, with the increments of fake Lévy area generated using some estimator $\widetilde{A}^{h_l}$.

2) The Brownian increments on the coarse path $Y_{l-1}^{\cdot,l}$ are computed by pairwise summing the increments of the fine path. The fake Lévy area used on the coarse path is computed using one iteration of Chen's identity applied to the increments and areas of the fine path.

This scheme however introduces a bias; namely, the distribution of the fake Lévy area used for the fine path at level l will not be the same as the distribution of Lévy area used for the coarse path at level $l + 1$. We may write the effect of this by amending the telescoping expectation to be

$$\sum_{l=1}^{L}\mathbb{E}\left[\varphi\left(Y_l(\widetilde{A}^{h_l})\right) - \varphi\left(Y_{l-1}(\widetilde{A}_{\text{CC}}^{h_l})\right)\right] = \underbrace{\sum_{l=1}^{L}\mathbb{E}\left[\varphi\left(Y_l(\widetilde{A}^{h_l})\right) - \varphi\left(Y_{l-1}(\widetilde{A}^{h_{l-1}})\right)\right]}_{\text{desired telescoping expectation}} \tag{14}$$

$$+ \underbrace{\sum_{l=1}^{L}\mathbb{E}\left[\varphi\left(Y_{l-1}(\widetilde{A}^{h_{l-1}})\right) - \varphi\left(Y_{l-1}(\widetilde{A}_{\text{CC}}^{h_l})\right)\right]}_{\text{bias term}}$$

where we have emphasised the dependence of the fine level on the fake area $\widetilde{A}^{h_l}$ and dependence of the coarse level of one Chen iteration of this fake area, denoted by $\widetilde{A}_{\text{CC}}^{h_l}$. The bias introduced is exactly the second sum. We aim to show empirically that this sum is small in comparison to the size of the weak error due to the SDE discretisation. In order to minimise this sum, the distribution of an estimator $\widetilde{A}$ must be as close as possible to the distribution Chen-combine($\widetilde{A}$); exactly the criterion used to train our generator.

17

The four numerical schemes in the comparison are: no-area Milstein, antithetic Milstein [GS14], the Strang splitting method, and a "Strang" log-ODE method. Only the final method incorporates the fake Lévy area. For details on the schemes see Section G.2. The first two schemes were included to demonstrate that the rate of variance reduction is comparable to two popular schemes, while the weak error rate of the Strang log-ODE method is (conjecture to be) $O(h^2)$ where the other methods achieve a weak error rate of $O(h)$. The numerical simulations were performed with a constant time-step h_l on each level satisfying $h_l = \frac{1}{2}h_{l-1}$. On the coarsest level we use the timestep $h_0 = \frac{1}{2}$ for the Milstein methods and $h_0 = 1$ for the Strang methods; this results in the variance on this level being approximately equal across the three methods. The number of sample paths on each level satisfies $n_l = \frac{1}{2}n_{l-1}$ with $n_0 = 2^{27}$, so the computational effort on each level is approximately constant. We repeat the experiment forty times and report the average result. We fix the log-Heston model parameters to be $T = 1$, $r = 0.1$, $K = 20$, $\kappa = 2$, $\theta = 0.1$, $\sigma = 0.5$, $U_0 = \log(20)$, and $V_0 = 0.4$.

The following plots report the multilevel variance defined by $\mathrm{Var}\left[\varphi\left(Y_l^{\cdot,l}\right) - \varphi\left(Y_{l-1}^{\cdot,l}\right)\right]$, and the empirical error given by $\left|\bar{\varphi}_{n_1,\ldots,n_l} - P_{\text{true}}\right|$, where P_{true} is the true price of the call option under the log-Heston model.

(a) Multilevel variance

(b) Empirical error

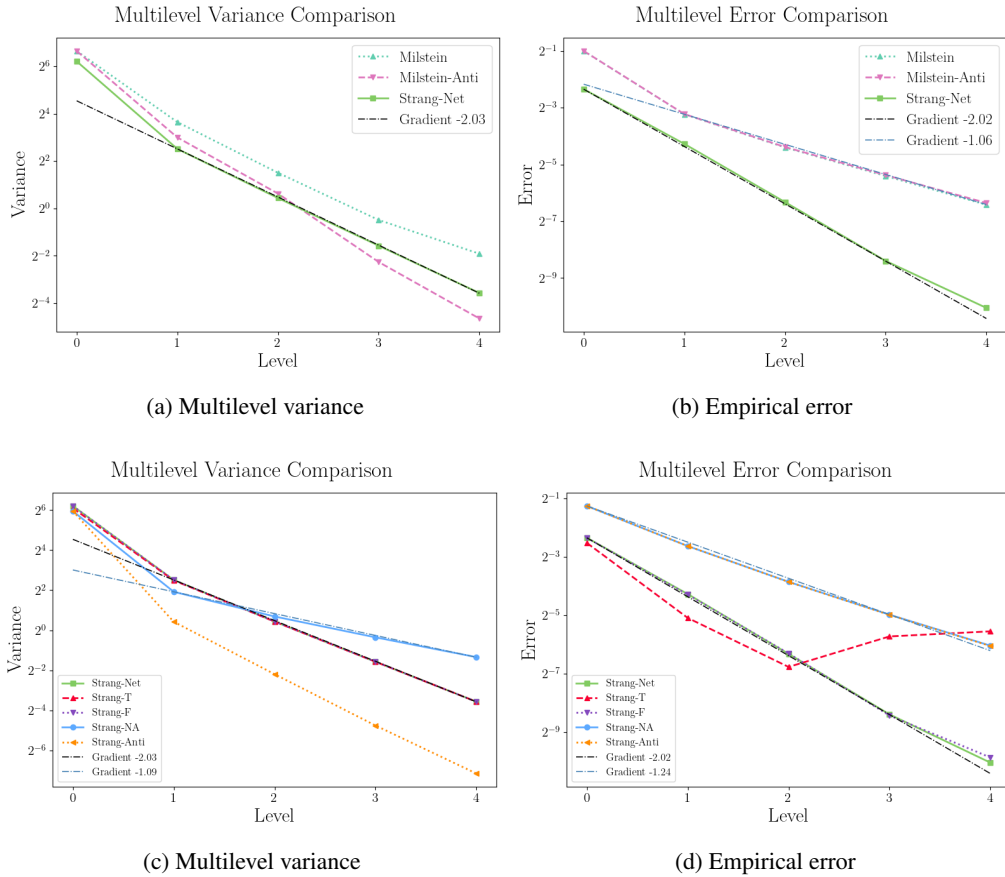(c) Multilevel variance

(d) Empirical error

Figure 6: Plots of multilevel variance and empirical error. The top pair of plots compare the Milstein scheme without area, Milstein antithetic and Strang log-ODE scheme with fake Lévy area from our generator (labelled "Strang-Net"). The bottom pair compare the Strang log-ODE scheme using three different fake Lévy areas. "Strang-T" indicates that the fake Lévy area is an independent Rademacher random variable with the correct variance (the same random variable appearing in the Talay scheme), and "Strang-F" denotes Foster's approximation. The "Strang-NA" line is the usual Strang splitting method with "Strang-Anti" being the antithetic version of this scheme.

In Figure 6a we see that the multilevel level variance of the Strang log-ODE method decreases at an approximate rate of $O(h^2)$. The rate for the Milstein antithetic scheme appears slightly higher, while the variance reduction rate for the standard Milstein method is clearly lower. As expected,

18

the weak convergence rate of both the Milstein and Milstein antithetic schemes is of order $O(h)$, while the weak rate for the Strang log-ODE with fake Lévy area is approximately $O(h^2)$. It was conjectured in [FRS24] that the Strang log-ODE method should attain this weak convergence rate, and the experiments corroborate this hypothesis.

When using a fake Lévy area in MLMC, a key factor for the performance of the scheme is how close the distribution of a Chen combined sample of Brownian motion and fake Lévy area is to the distribution before performing the combine operation. Since we employed Chen training, our model succeeds in matching the distributions well enough to match and even outperform Foster's method. In Table 3, we record the bias introduced at each level, as in Equation (14), for each fake Lévy area.

Level	0	1	2	3
Strang-Net (10^{-3})	-0.402	0.313	-0.133	-0.652
Strang-F (10^{-3})	0.361	0.848	0.0714	1.31
Strang-T (10^{-3})	-17.0	4.33	-1.79	-1.10

Table 3: Approximate bias introduced per level by the use of different fake Lévy areas. We use 2^{29} samples paths on each level.

For LévyGAN and Foster's method, the bias introduced on each level of the telescoping sum is of order 2^{-11}; this is far smaller than the weak error seen in Figure 6d. However, it is possible that the accumulated bias may then be of order 2^{-9} on the finest level, which may account in part for the slight deviation from the line at level 4. It is also clear that it is not enough for the fake Lévy area simply to match the mean and variance of true Lévy area, as demonstrated by the poor performance of the "Strang-T" method. However, we do note here that a scheme matching the conditional variance of Lévy area given a Brownian increment performed similarly to Foster's method in previous experiments. We may also see from the performance of the Strang splitting method that, without the fake Lévy area terms, one achieves only a weak order convergence rate of $O(h)$. It is interesting to note however, that Figure 6c indicates that the fake Lévy area need only match the mean and variance of true Lévy area to obtain improved variance reduction at each level. Even the "Strang T" method has the same variance reduction rate as the more sophisticated techniques despite having poor empirical error.

In practice, one usually wishes to obtain some target root mean-squared error (RMSE) with minimal computational cost. In this setting, for two numerical schemes with variance reduction $O(h^\beta)$ with $\beta > 1$, the scheme with higher order weak convergence is not necessarily the preferred one. By the complexity theorem of Giles [Gil08, Theorem 3.1], the optimal number of sample paths on each level should be asymptotically proportional to $O(h_l^{(\beta+1)/2})$. As such, the computational effort should be expended mostly on the coarse levels in the regime $\beta > 1$, driving one towards discretisations that are computationally cheap on the lower levels. Since it is difficult measure the computational complexity of the Strang log-ODE scheme with fake Lévy area produced by a generative model, we use the following approach. We implement the algorithm of Giles [Gil08, Section 5] for the Milstein scheme and Strang log-ODE scheme and compare the average time taken to achieve a selection of target RMSEs between 0.1 and 0.0025.

RMSE	0.1	0.0441	0.0129	0.0086	0.0057	0.0038	0.0025
Milstein (s)	**0.0097**	0.0256	0.376	1.03	2.86	8.63	23.6
LévyGAN (s)	0.0102	**0.0128**	**0.142**	**0.311**	**0.806**	**2.25**	**5.83**

Table 4: The average time taken across 25 runs for the Milstein and Strang log-ODE methods to attain a target RMSE. We use the algorithm of [Gil08, Section 5] to determine the number of samples on each level and the stopping condition on the number of levels used on each run. All random variables are generated in `torch` on GPU, with the numerical schemes implemented in `numpy` on CPU.

19

Remark 6.1. We see from Figure 6c that the the Strang-antithetic scheme achieves the highest order variance reduction with a first order weak error rate. As noted above, both factors play a role in the overall time required to achieve a desired RMSE and it is possible that the higher order variance reduction of the Strang-antithetic scheme may outperform the high order weak error of the LévyGAN based approach. However, it was recently shown in [Igu+25] that the antithetic method can be combined with weak estimators of Lévy area to achieve high order variance reduction. We believe that combining their approach with ours would result in a scheme with both high order variance reduction and weak error rate.

We conclude this section by reiterating that the use of extra random variables to attain higher order weak convergence has become a popular technique, see for example [Tal90; NV08; NN09]. But, to the best of our knowledge, it has not yet been observed that the use of fake Lévy area combined with standard multilevel Monte-Carlo can also achieve high order weak convergence and variance reduction.

7 Generating other integrals of Brownian motion

To demonstrate the wider applicability of the Chen-training paradigm, we turn our attention to generating the integral $C_{s,t} = \int_s^t W_{s,r}^2 \, dr$ where W is a 1-dimensional Brownian motion. While a detailed discussion of this integral is beyond the scope of this paper, we note that numerical methods for scalar noise SDEs can achieve second order strong convergence if this integral is provided alongside Brownian increments and space-time Lévy areas (see [FLO20; TX19] for further details).

Analogous to the procedure outlined in this article for the generation of space-space Lévy area, we may attempt to train a network to sample from the distribution $\mathbb{P}_{C_{0,1}|W_{0,1}=w, \, H_{0,1}=h}$, where H is the space-time Lévy area defined in Definition 3.1. Due to Brownian scaling, the distribution of $C_{0,1}$ satisfies the following scale invariance and modified Chen's relation.

Proposition 7.1 (Scaling and Chen's relation for C). *Let W and C be defined as above and $0 \le s < t$. Then*

$$C_{s,t} \stackrel{d}{=} (t-s)^2 C_{0,1} \quad and \quad C_{0,1} = C_{0,\frac{1}{2}} + C_{\frac{1}{2},1} + W_{0,\frac{1}{2}} \left(\frac{W_{0,1}}{2} + H_{\frac{1}{2},1} \right).$$

We note that, since $C_{0,1}$ is 1-dimensional and non-negative, neither Pair-Net nor bridge-flipping are required. We can then train a feed-forward neural network with 2 hidden layers; 16 hidden dimensions; Gaussian noise of dimension 3 in addition to w and h; ReLU activation function; and the absolute value applied to the output to maintain positivity. We then train using the Chen relation described in the preceding. To compare our output, generated "true samples" for fixed pairs (w, h) by taking fine discretisation of $\int_s^t W_{s,r}^2 \, dr$ using the Diffrax library [Kid21].

Our method achieved a 2-Wasserstein error of 3.27×10^{-5}. Just as for space-space Lévy area, we can generate a Gaussian variable with the correct conditional mean and variance (see [FLO20]). However, this achieved a 2-Wasserstein error of 7.67×10^{-4}; twenty times higher than our error. This experiment demonstrates that the Chen-training approach is not only limited to Lévy area, but applicable to other integrals of Brownian motion that have relevance in the numerical SDE simulation.

8 Conclusion and Open Directions

While stochastic analysis techniques are often used in generative deep learning, this article appears to be one of the first examples where deep learning methodology has provided meaningful results in an application to stochastic analysis. Indeed, we have demonstrated a proof of concept that the techniques used in LévyGAN have a place in the field of numerical solutions to SDEs. We remark here though, that careful consideration of the domain-specific analytical properties was required. In particular, regardless of the network size or architecture, LévyGAN in its initial form was an order of magnitude less accurate without the inclusion of both bridge-flipping and Pair-net.

One open direction for future research is a careful analysis of the conditions required by the fake Lévy area in order to achieve optimal convergence rates in multilevel Monte Carlo. For example, we expect that fake Lévy area could be incorporated into antithetic MLMC schemes, such as [Igu+25].

An application of particular interest would be a GAN-based adaptive SDE solver. That is, a method that first generates a coarsely discretised path, before checking whether the step-size of the solver should be reduced. Such functionality is desirable for use in Neural SDEs [Li+20b; Kid+21a; Kid+21b] and Logsig-RNN generators [Ni+21], which are both powerful methods for modelling noisy time series data. In the context of Lévy area generation, this would require the ability to generate Lévy area and Brownian increments over two half intervals given the Lévy area and Brownian increment over the larger interval. One approach would be to use the analytical characteristic function given in [GQ12] which provides the joint characteristic function evaluated at multiple time points. However, we expect the training time to be rather long, since the evaluation of the characteristic function involves solving a recursive system of matrix Ricatti equations in addition to a system of independent linear matrix ODEs of order one.

Finally, it is possible to extend the Chen-training approach. This might take several forms: one might derive a Chen type relation for higher order terms in the polynomial expansion of Brownian motion (e.g. for H and b) as in Section 7; use the ordinary Chen's relation for the generation of higher order terms in the log-signature of Brownian motion; generating Lévy areas for certain Lévy processes.

For the third application, our approach may be applicable to the generation of Lévy areas of α-stable Lévy processes, where moment matching approaches are not possible, since these processes have unbounded variance for $\alpha < 2$. Indeed, the α-stable Lévy process X_t^α satisfies the scaling property $X_t^\alpha = t^{1/\alpha} X_1^\alpha$ in addition to independent and stationary increments. Combining these properties together, the distribution of its Lévy area (defined using Itô integration with jumps) should also be invariant under a suitably re-scaled version of Chen's relation. One could then attempt to train a network under this Chen relation, analogous to our approach for Brownian motion.

Acknowledgements

References

[BFH09]   E. Breuillard, P. Friz, and M. Huesmann. "From random walks to rough paths". In: *Proceedings of the American Mathematical Society* 137.10 (2009), pp. 3487–3496.

[Bro+20] A. Browning, D. Warne, K. Burrage, R. Baker, and M. Simpson. "Identifiability analysis for stochastic differential equation models in systems biology". In: *Journal of the Royal Society Interface* 17.173 (2020).

[CC80]   J. M. C. Clark and R. J. Cameron. "The maximum rate of convergence of discrete approximations for stochastic differential equations". In: *Stochastic Differential Systems Filtering and Control*. Springer Berlin Heidelberg, 1980, pp. 162–171.

[Che57]   K.-T. Chen. "Integration of Paths, Geometric Invariants and a Generalized Baker- Hausdorff Formula". In: *Annals of Mathematics* 65.1 (1957), pp. 163–178.

[CL16]   I. Chevyrev and T. Lyons. "Characteristic functions of measures on geometric rough paths". In: *The Annals of Probability* 44.6 (2016), pp. 4049–4082.

[Cri15]   R. Crisostomo. *An Analysis of the Heston Stochastic Volatility Model: Implementation and Calibration using Matlab*. 2015. arXiv: 1502.02963.

[Csö81a] S. Csörgő. "Limit Behaviour of the Empirical Characteristic Function". In: *The Annals of Probability* 9.1 (1981), pp. 130–144.

[Csö81b] S. Csörgő. "Multivariate empirical characteristic functions". In: *Zeitschrift für Wahrscheinlichkeitheorie und Verwandte Gebiete* 55.2 (1981), pp. 203–229.

[Dav14]   A. Davie. "KMT Theory Applied to Approximations of SDE". In: *Stochastic Analysis and Applications 2014*. Springer, 2014, pp. 185–201.

[Dic07]   A. S. Dickinson. "Optimal Approximation of the Second Iterated Integral of Brownian Motion". In: *Stochastic Analysis and Applications* 25.5 (2007), pp. 1109–1128.

[FH22]   J. Foster and K. Habermann. "Brownian bridge expansions for Lévy area approximations and particular values of the Riemann zeta function". In: *Combinatorics, Probability and Computing* (2022), pp. 1–28.

[FL15]   G. Flint and T. Lyons. *Pathwise approximation of SDEs by coupling piecewise abelian rough paths*. 2015. arXiv: 1505.01298.

[FLO20]   J. Foster, T. Lyons, and H. Oberhauser. "An optimal polynomial approximation of Brownian motion". In: *SIAM Journal on Numerical Analysis* 58.3 (2020), pp. 1393–1421.

[FM77]   A. Feuerverger and R. Mureika. "The Empirical Characteristic Function and Its Applications". In: *The Annals of Statistics* 5.1 (1977), pp. 88–97.

[Fos20]   J. Foster. "Numerical approximations for stochastic differential equations". PhD thesis. University of Oxford, 2020.

[Fos25]   J. Foster. "Approximating the signature of Brownian motion for high order SDE simulation". In: *Stochastic Analysis and Applications 2025*. Springer, 2025.

[FRS24]   J. Foster, G. dos Reis, and C. Strange. "High order splitting methods for SDEs satisfying a commutativity condition". In: *SIAM Journal on Numerical Analysis* 62.1 (2024), pp. 500–532.

[FSS20]   A. Fatir Ansari, J. Scarlett, and H. Soh. "A Characteristic Function Approach to Deep Implicit Generative Modeling". In: *2020 IEEE/CVF Conference on Computer Vision and Pattern Recognition (CVPR)*. 2020.

[Gil08]   M. B. Giles. "Multilevel Monte Carlo Path Simulation". In: *Operations research* 56.3 (2008), pp. 607–617.

[GL94]   J. Gaines and T. Lyons. "Random Generation of Stochastic Area Integrals". In: *SIAM Journal on Applied Mathematics* 54.4 (1994), pp. 1132–1146.

[Goo+14]   I. Goodfellow, J. Pouget-Abadie, M. Mirza, B. Xu, D. Warde-Farley, S. Ozair, A. Courville, and Y. Bengio. "Generative Adversarial Nets". In: *Advances in Neural Information Processing Systems*. Vol. 27. 2014.

[GQ12]   X. Geng and Z. Qian. *On the Finite Dimensional Joint Characteristic Function of Lévy's Stochastic Area Processes*. 2012. arXiv: 1206.1241.

[Gre81]   W. H. Greub. "Linear Algebra". In: (1981).

[GS14]   M. B. Giles and L. Szpruch. "Antithetic multilevel Monte Carlo estimation for multidimensional SDEs without Lévy area simulation". In: *The Annals of Applied Probability* 24.4 (2014), pp. 1585–1620.

[HS83]   K. Helmes and A. Schwane. "Lévy's stochastic area formula in higher dimensions". In: *Journal of Functional Analysis* (1983).

[Igu+25]   Y. Iguchi, A. Jasra, M. Maama, and A. Beskos. "Antithetic Multilevel Methods for Elliptic and Hypoelliptic Diffusions with Applications". In: *SIAM/ASA Journal on Uncertainty Quantification* 13.2 (2025), pp. 805–830.

[Kid+21a] P. Kidger, J. Foster, X. Li, and T. Lyons. "Efficient and Accurate Gradients for Neural SDEs". In: *Advances in Neural Information Processing Systems*. Vol. 34. 2021, pp. 18747–18761.

[Kid+21b] P. Kidger, J. Foster, X. Li, and T. J. Lyons. "Neural SDEs as Infinite-Dimensional GANs". In: *Proceedings of the 38th International Conference on Machine Learning*. Vol. 139. Proceedings of Machine Learning Research. PMLR, 2021, pp. 5453–5463.

[Kid21]   P. Kidger. "On Neural Differential Equations". PhD thesis. University of Oxford, 2021.

[KP92]   P. Kloeden and E. Platen. *Numerical solution of stochastic differential equations*. Applications of Mathematics, Stochastic Modelling and Applied Probability, 23. Springer-Verlag, 1992.

[KPW92]   P. Kloeden, E. Platen, and I. Wright. "The approximation of multiple stochastic integrals". In: *Stochastic Analysis and Applications* 10.4 (1992), pp. 431–441.

[KR23]   F. Kastner and A. Rößler. "An Analysis of Approximation Algorithms for Iterated Stochastic Integrals and a Julia and MATLAB Simulation Toolbox". In: *Numerical Algorithms* 93 (2023), pp. 27–66.

[LCL07]   T. J. Lyons, M. Caruana, and T. Lévy. *Differential Equations Driven by Rough Paths. Ecole d'Eté de Probabilités de Saint-Flour XXXIV-2004*. Springer Berlin, Heidelberg, 2007.

[Li+19]   X. Li, D. Wu, L. Mackey, and M. A. Erdogdu. "Stochastic Runge-Kutta Accelerates Langevin Monte Carlo and Beyond". In: *Advances in Neural Information Processing Systems* (2019).

[Li+20a]   S. Li, Z. Yu, M. Xiang, and D. Mandic. "Reciprocal adversarial learning via characteristic functions". In: *Advances in Neural Information Processing Systems*. Vol. 33. 2020, pp. 217–228.

[Li+20b]   X. Li, T.-K. L. Wong, R. T. Q. Chen, and D. K. Duvenaud. "Scalable Gradients and Variational Inference for Stochastic Differential Equations". In: *Proceedings of The 2nd Symposium on Advances in Approximate Bayesian Inference*. Vol. 118. 2020, pp. 1–28.

[LLN23]   H. Lou, S. Li, and H. Ni. "PCF-GAN: generating sequential data via the characteristic function of measures on the path space". In: *Advances in Neural Information Processing Systems*. Vol. 36. 2023, pp. 39755–39781.

[LM15]   B. Leimkuhler and C. Matthews. *Molecular Dynamics: With Deterministic and Stochastic Numerical Methods*. Interdisciplinary Applied Mathematics, Springer, 2015.

[LNT24]   T. Lyons, H. Ni, and J. Tao. *A PDE approach for solving the characteristic function of the generalised signature process*. 2024. arXiv: 2401.02393.

[Loè78]   M. Loève. *Probability theory II*. Fourth edition. Graduate texts in mathematics ; 46. Springer, 1978.

[MO14]   M. Mirza and S. Osindero. *Conditional Generative Adversarial Nets*. 2014. arXiv: 1411.1784.

[MR22]   J. Mrongowius and A. Rößler. "On the approximation and simulation of iterated stochastic integrals and the corresponding Lévy areas in terms of a multidimensional Brownian motion". In: *Stochastic Analysis and Applications* 40.3 (2022), pp. 397–425.

[MT04]   G. N. Milstein and M. V. Tretyakov. *Stochastic Numerics for Mathematical Physics*. Berlin, Heidelberg: Springer Berlin Heidelberg, 2004.

[MW14]   S. J. A. Malham and A. Wiese. "Efficient almost-exact Lévy area sampling". In: *Statistics & Probability Letters* 88 (2014), pp. 50–55.

[Ni+21]   H. Ni, L. Szpruch, M. Sabate-Vidales, B. Xiao, M. Wiese, and S. Liao. "Sig-Wasserstein GANs for time series generation". In: *Proceedings of the Second ACM International Conference on AI in Finance*. 2021, pp. 1–8.

[NN09]   M. Ninomiya and S. Ninomiya. "A new higher-order weak approximation scheme for stochastic differential equations and the Runge–Kutta method". In: *Finance and Stochastics* 13.3 (2009), pp. 415–443.

[NV08]   S. Ninomiya and N. Victoir. "Weak Approximation of Stochastic Differential Equations and Application to Derivative Pricing". In: *Applied Mathematical Finance* 15.2 (2008), pp. 107–121.

[PT85]   E. Pardoux and D. Talay. "Discretization and simulation of stochastic differential equations". In: *Acta Applicandae Mathematica* 3.1 (1985), pp. 23–47.

[Röß09]   A. Rößler. "Second Order Runge–Kutta Methods for Itô SDEs". In: *SIAM Journal on Numerical Analysis* 47.3 (2009), pp. 1713–1738.

[Sca+09]   F. Scarselli, M. Gori, A. C. Tsoi, M. Hagenbuchner, and G. Monfardini. "The Graph Neural Network Model". In: *IEEE Transactions on Neural Networks* 20.1 (2009).

[Shr04]   S. Shreve. *Stochastic Calculus for Finance II: Continuous-Time Models*. Springer, 2004.

[Sri+10]   B. Sriperumbudurm, A. Gretton, K. Fukumizu, B. Schölkopf, and G. Lanckriet. "Hilbert Space Embeddings and Metrics on Probability Measures". In: *Journal of Machine Learning Research* 11.50 (2010), pp. 1517–1561.

[Tal90]   D. Talay. "Second-order discretization schemes of stochastic differential systems for the computation of the invariant law". In: *Stochastics and Stochastic Reports* 29.1 (1990).

[Ter22]   K. Terada. *Higher order methods and Multilevel Monte Carlo for SDEs in Finance*. Masters thesis, University of Edinburgh. 2022.

[TX19]   X. Tang and A. Xiao. "Asymptotically optimal approximation of some stochastic integrals and its applications to the strong second-order methods". In: *Advances in Computational Mathematics* 45 (2019), pp. 813–846.

[Wik01]   M. Wiktorsson. "Joint characteristic function and simultaneous simulation of iterated Itô integrals for multiple independent Brownian motions". In: *The Annals of Applied Probability* 11.2 (2001), pp. 470–487.

A   Some Properties of the CFD

This short subsection summarises two key properties of the distance CFD_Λ. Namely, the following proposition shows that the distance between the empirical characteristic function and true characteristic function converges to zero almost surely as the number of observations tends to infinity. The second result demonstrates that by carefully choosing $\Lambda \sim \nu$, convergence in CFD_Λ implies weak convergence.

Proposition A.1. *Let $\{X_i\}_{i=1}^\infty$ be a collection of i.i.d. $\mathbb{R}^n$ valued random variables, then*

$$\lim_{n \to \infty} \mathbb{E}_{\Lambda \sim \nu}\Big[\big|\widehat{\Phi}_X^n(\Lambda) - \Phi_X(\Lambda)\big|\Big] \to 0 \ \ \text{almost-surely.}$$

Proof. By [FM77; Csö81a; Csö81b], there exists a sequence of real numbers $\{T_n\} \uparrow \infty$ such that almost-surely for every $\varepsilon > 0$ there exists an N such that for every $n \geq N$

$$\sup_{|\Lambda| \leq T_n} \Big|\widehat{\Phi}_X^n(\Lambda) - \Phi_X(\Lambda)\Big| < \varepsilon.$$

It follows almost-surely for every $\varepsilon > 0$ that

$$
\begin{aligned}
\mathbb{E}_{\Lambda \sim \nu}\Big[\big|\widehat{\Phi}_X^n(\Lambda) - \Phi_X(\Lambda)\big|\Big] &= \int \big|\widehat{\Phi}_X^n(\Lambda) - \Phi_X(\Lambda)\big| d\nu(\Lambda) \\
&\leq \int_{|\Lambda| \leq T_n} \big|\widehat{\Phi}_X^n(\Lambda) - \Phi_X(\Lambda)\big| d\nu(\Lambda) + 2\nu(\{|\Lambda| \geq T_n\}) \\
&\leq \varepsilon\nu(\{|\Lambda| \leq T_n\}) + 2\nu(\{|\Lambda| \geq T_n\}) \\
&\to \varepsilon.
\end{aligned}
$$

$\square$

Proposition A.2. *Let ν be the Cauchy distribution on $\mathbb{R}^n$ with location parameter 0 scale parameter γ and independent coordinates, then $\text{CFD}_{\Lambda \sim \mu}$ metrizes the topology of weak convergence on $\mathcal{P}(\mathbb{R}^n)$.*

Proof. We consider the case $n = 1$; the general case is a straightforward extension. If the law of a random variable T is that of a Cauchy distribution with location parameter 0 and scale parameter γ, then it is well known that its characteristic function is given by

$$\Phi_T(t) = e^{-\gamma|t|},$$

and has a density given by

$$f_T(x) = \frac{1}{2\pi}\int_{\mathbb{R}} e^{-itx}\Phi_T(t)\,dt = \frac{1}{\pi\gamma\left(1 + \left(\frac{x}{\gamma}\right)^2\right)}.$$

It is clear that both Φ_T and f_T are in $L^1(\mathbb{R})$, since

$$\int_{\mathbb{R}} \Phi_T(t)\,dt = \frac{2}{\gamma}, \ \text{and} \ \int_{\mathbb{R}} f_T(x)\,dx = 1.$$

We also observe that

$$\int_{\mathbb{R}} \frac{1}{f_T(x)(1 + |x|^4)}\,dx \leq 2\pi\gamma \int_0^\infty \frac{\left(1 + \frac{|x|}{\gamma}\right)^2}{(1 + |x|)^4}\,dx < \infty.$$

An application of [Sri+10], the uniform boundedness of characteristic functions in $L^\infty(\mu)$, and a standard interpolation argument yields that $\text{CFD}_{\Lambda \sim \mu}$ metrizes weak convergence. $\square$

24

A.1 Proof of the Second-order polynomial Expansion

Proof. The Browninan bridge B and increment $W_{s,t}$ are independent, hence so are $\{H_{s,u}\}_{u\in[s,t]}$ and $\{b_{s,u}\}_{u\in[s,t]}$. This is because $B_u = W_{s,u} - \frac{u-s}{t-s}W_{s,t}$, and $W_{s,t}$ are jointly Gaussian and $\mathrm{cov}(B_u, W_{s,t}) = (u-s) - \frac{u-s}{t-s}(t-s) = 0$ for all $u \in [s,t]$, so they are independent.

To prove the second assertion, recall that an integral of a Gaussian process is Gaussian. Therefore, H is Gaussian. Since $H^{(i)}$ only depends on $W^{(i)}$ and $W^{(i)}$ and $W^{(j)}$ are independent for $j \neq i$ (by definition), the coordinates of H are independent. Since $H_{s,t} \overset{d}{=} H_{0,t-s}$ we only need to determine the mean and variance of H_t.

$$\mathbb{E}\big[H_t^{(i)}\big] = \mathbb{E}\left[\frac{1}{t}\int_0^t W_{0,u} - \frac{u}{t}W_t \, du\right] = \frac{1}{t}\int_0^t \mathbb{E}\left[W_{0,u} - \frac{u}{t}W_t\right] du = 0.$$

Integration by parts gives

$$tW_t^{(i)} = \int_0^t s\,dW_s^{(i)} + \int_0^t W_s^{(i)}\,ds \implies \frac{1}{t}\int_0^t W_s^{(i)}\,ds = W_t^{(i)} - \frac{1}{t}\int_0^t s\,dW_s^{(i)}$$

$$H_t^{(i)} = \frac{1}{t}\int_0^t W_s^{(i)} - \frac{s}{t}W_t^{(i)}\,ds = \frac{1}{t}\int_0^t W_s^{(i)}\,ds - \frac{1}{2}W_t^{(i)} = \frac{1}{2}W_t^{(i)} - \frac{1}{t}\int_0^t s\,dW_s^{(i)}.$$

Since $\mathbb{E}\big[(W_t)^2\big] = t$ and $H_t \perp W_t$ we obtain

$$\begin{aligned}
\mathbb{E}\left[\left(H_t^{(i)}\right)^2\right] &= \mathbb{E}\left[\left(H_t^{(i)}\right)^2\right] + \frac{1}{4}\mathbb{E}\left[\left(W_t^{(i)}\right)^2\right] - \frac{t}{4} \\
&= \mathbb{E}\left[\left(\frac{1}{2}W_t^{(i)} - H_t^{(i)}\right)^2\right] - \frac{t}{4} = \mathbb{E}\left[\left(\frac{1}{t}\int_0^t s\,dW_s^{(i)}\right)^2\right] - \frac{t}{4} \\
&= \frac{1}{t^2}\mathbb{E}\left[\left\langle\int_0^t s\,dW_s^{(i)}\right\rangle\right] - \frac{t}{4} = \frac{1}{t^2}\mathbb{E}\left[\int_0^t s^2\,d\langle W_s^{(i)}\rangle\right] - \frac{t}{4} \\
&= \frac{1}{t^2}\mathbb{E}\left[\int_0^t s^2\,ds\right] - \frac{t}{4} = \frac{1}{12}t.
\end{aligned}$$

$\square$

Proof. We will prove the decomposition for $A_{0,1}$, which can be extended to the general case by scaling. If B is the Brownian bridge on $[0,1]$, then for $t \in [0,1]$ $W_t = tW_1 + B_t$, so

$$\begin{aligned}
A_{s,t}^{(i,j)} &= \int_0^1 W_t^{(i)}\,dW_t^{(j)} - \frac{1}{2}W_1^{(i)}W_1^{(j)} \\
&= \int_0^1 \left(tW_1^{(i)} + B_t^{(i)}\right) d\left(tW_1^{(j)} + B_t^{(j)}\right) - \frac{1}{2}W_1^{(i)}W_1^{(j)} \\
&= \frac{1}{2}W_1^{(i)}W_1^{(j)} + W_1^{(j)}\int_0^1 B_t^{(i)}\,dt + W_1^{(i)}\int_0^1 t\,dB_t^{(j)} + \int_0^1 B_t^{(i)}\,dB_t^{(j)} - \frac{1}{2}W_1^{(i)}W_1^{(j)} \\
&= W_1^{(j)}H_1^{(i)} + W_1^{(i)}\int_0^1 t\,dB_t^{(j)} + b_{0,1}^{(i,j)}
\end{aligned}$$

we use stochastic integration by parts and the fact that $B_1 = 0$ to get

$$tB_t^{(j)} = \int_0^t s\,dB_s^{(j)} + \int_0^t B_s^{(j)}\,ds \implies \int_0^1 t\,dB_t^{(j)} = -\int_0^1 B_t^{(j)}\,dt = -H_1^{(j)}.$$

Plugging this into the above equality gives $A_{s,t}^{(i,j)} = H_{s,t}^{(i)}W_{s,t}^{(j)} - W_{s,t}^{(i)}H_{s,t}^{(j)} + b_{s,t}^{(i,j)}$ as required. $\square$

B Proof of the Chen-Uniqueness Theorem

Here we present the proofs of our main theoretical contributions. Firstly, we prove that the joint law of a Brownian increment and its Lévy area is the unique distribution that is invariant under an iteration of the Chen-combine operation.

Theorem B.1 (Distributional uniqueness of Lévy area under Chen's relation). *Suppose μ is a mean zero probability distribution on $\mathbb{R}^d \times \mathbb{R}^{d \times d}$, where the first marginal has finite second moment. Let $(V_i, Z_i) \overset{i.i.d.}{\sim} \mu$ for $i = 1, 2$; if it holds that*

$$V_3 := \tfrac{1}{\sqrt{2}} (V_1 + V_2), \quad Z_3 := \tfrac{1}{2} Z_1 + \tfrac{1}{2} Z_2 + \tfrac{1}{4} (V_1 \otimes V_2 - V_2 \otimes V_1) \tag{15}$$

is also distributed according to μ, then μ is the distribution of $(W_{0,1}, A_{0,1})$ where A is the Lévy area process associated with a d-dimensional Brownian motion W.

Proof. Let $(\Omega, \mathcal{F}, \mathbb{P})$ be a probability space carrying for each $N \in \mathbb{N}$ a sequence of random variables $(V_i^{N,N}, Z_i^{N,N})_{i=1}^{2^N} \overset{i.i.d.}{\sim} \mu$. For each N define via backward recursion the sequences $(V_i^{k,N}, Z_i^{k,N})_{i=1}^{2^k}$ for $k = 0, 1, \ldots, N-1$ by

$$V_i^{k,N} = \frac{1}{\sqrt{2}} (V_{2i-1}^{k+1,N} + V_{2i}^{k+1,N}) \quad \text{and} \tag{16}$$

$$Z_i^{k,N} = \frac{1}{2} (V_{2i-1}^{k+1,N} + V_{2i}^{k+1,N}) + \frac{1}{4} (V_{2i-1}^{k+1,N} \otimes V_{2i}^{k+1,N} - V_{2i}^{k+1} \otimes V_{2i-1}^{k+1,N}). \tag{17}$$

Using the assumptions on μ, it follows that $(V_i^{k,N}, Z_i^{k,N})_{i=1}^{2^k} \overset{i.i.d.}{\sim} \mu$ for every k. We now define

$$X_k^N = \left(\frac{1}{2^{k/2}} \sum_{i=1}^{2^k} V_i^{k,N}, \frac{1}{2^n} \sum_{i=1}^{2^k} Z_i^{k,N} \right) \quad \text{for } k = 0, \ldots, N, \tag{18}$$

noting that $X_0^N = (V_1^{0,N}, Z_1^{0,N}) \sim \mu$. For every N we have the telescoping sum

$$X_0^N = \sum_{k=1}^{N-1} (X_{k-1}^N - X_k^N) + X_N^N,$$

and since by Equations (16) and (17)

$$X_{k-1}^N - X_k^N = \frac{1}{2^{k+1}} \left(0, \sum_{i=1}^{2^{k-1}} V_{2i-1}^{k,N} \otimes V_{2i}^{k,N} - V_{2i}^{k,N} \otimes V_{2i-1}^{k,N} \right),$$

this relation may be rewritten as

$$X_0^N = \left(\frac{1}{2^{N/2}} \sum_{i=1}^{2^N} V_i^{N,N}, \sum_{k=1}^{N} \frac{1}{2^{k+1}} \sum_{i=1}^{2^{k-1}} V_{2i-1}^{k,N} \otimes V_{2i}^{k,N} - V_{2i}^{k,N} \otimes V_{2i-1}^{k,N} \right)$$

$$+ \left(0, \frac{1}{2^N} \sum_{i=1}^{2^N} Z_i^{N,N} \right).$$

The left-hand side has distribution μ independent of N, while on the right-hand side the second term tends to zero in probability, while the first term can be recognised as having the distribution

$$(W_{0,1}^{D_N}, \text{Area}(W_{0,1}^{D_N})) \overset{d}{\to} (W_{0,1}, A_{0,1}) \quad \text{as } N \to \infty,$$

where W^{D_N} is the piecewise linear interpolation of a rescaled random walk along the Nth diadic partition D_N of $[0, 1]$. Here $\text{Area}(W_{0,1}^{D_N})$ denotes the Lévy area of the piecewise linear interpolation. The convergence in distribution follows from Donsker's theorem for enhanced Brownian motion [BFH09, Theorems 2 and 3]. The proof is concluded by an application of Slutsky's theorem. $\quad\square$

Remark B.2. To see that

$$\sum_{k=1}^{N} \frac{1}{2^{k+1}} \sum_{i=1}^{2^{k-1}} V_{2i-1}^{k,N} \otimes V_{2i}^{k,N} - V_{2i}^{k,N} \otimes V_{2i-1}^{k,N}$$

has the distribution of the Lévy area of the piecewise linear approximation of Brownian motion on the diadic partition D^N, one can note that for each $k = 1, \ldots, N$, the summand is the signed area between the piecewise linear approximation on D^k and the piecewise linear approximation on the coarser partition D^{k-1}. For a piecewise linear path, the Lévy area is given by the sum of these enclosed areas. Alternatively, one can show via induction that the sum may be rearranged to give the trapezium rule applied on D^N to the Lévy area of the piecewise linear approximation on the same partition. The trapezium rule in this case will be exact.

If one additionally assumes that the distribution μ has finite variance and that the first marginal is Gaussian, then an alternative proof is possible utilising Wasserstein distances.

Theorem B.3 (Distributional Uniqueness of Lévy area under Chen's relation (finite variance))**.** *Suppose a distribution μ on $\mathbb{R}^d \times \mathbb{R}^{d \times d}$ has the following properties:*

(i) *If $(V, Z) \sim \mu$, where $V \in \mathbb{R}^d$, $Z \in \mathbb{R}^{d \times d}$, then*

- $V \sim \mathcal{N}^d(0, 1)$,
- $\mathbb{E}[Z] = 0$,
- $\mathrm{var}(Z) < \infty$;

(ii) *If $(V_1, Z_1), (V_2, Z_2) \sim \mu$, are i.i.d. tuples, and we define*

$$V_3 := \tfrac{1}{\sqrt{2}} (V_1 + V_2), \quad Z_3 := \tfrac{1}{2} Z_1 + \tfrac{1}{2} Z_2 + \tfrac{1}{4} (V_1 \otimes V_2 - V_2 \otimes V_1), \qquad (19)$$

then $(V_3, Z_3) \sim \mu$.

Then μ is the distribution of $(W_{0,1}, A_1)$ where A is the Lévy area process associated with a d-dimensional Brownian motion W.

Proof. Denote the distribution of $(W_{0,1}, A_1)$ by ν. We will try to estimate the 2-Wasserstein metric $\mathcal{W}_2(\mu, \nu)$, and show that it is 0. Since $\mathcal{W}_2$ is a metric, that means that $\mu = \nu$. Since the Wasserstein metric is defined using an infimum over all couplings γ, an upper bound on it can be obtained by picking a particular coupling and computing the L^2 distance between (Z, V) and $(A_{0,1}, W_1)$ under that coupling.

Let $K \in \mathbb{N}$ be a number and let (Z_n^K, V_n^K) (for $n = 1, 2, \ldots, 2^K$) be independent random variables drawn from μ (the superscript K is an index, not a power). We will repeatedly apply (19) in a binary-tree fashion to combine all of these random variables into (Z_1^0, V_1^0). Provided we are at layer $k \geq K$, consisting of $\{(Z_n^k, V_n^k) : 1 \leq n \leq 2^k\}$, we can produce layer $k - 1$ by setting

$$Z_n^{k-1} := \tfrac{1}{2} Z_{2n-1}^k + \tfrac{1}{4} Z_{2n}^k + \tfrac{1}{2} \left(V_{2n-1}^k \otimes V_{2n}^k - V_{2n}^k \otimes V_{2n-1}^k \right),$$

$$V_n^{k-1} := \tfrac{1}{\sqrt{2}} \left(V_{2n-1}^k + V_{2n}^k \right).$$

If the random variables $\{(Z_n^k, V_n^k) : 1 \leq n \leq 2^k\}$ are independent and μ-distributed, then by (ii), so are $\{(Z_n^{k-1}, V_n^{k-1}) : 1 \leq n \leq 2^{k-1}\}$. By induction we conclude that $(Z_1^0, V_1^0) \sim \mu$.

Furthermore, Z_1^0 can be decomposed into a sum

$$Z_1^0 = D + \sum_{n=1}^{2^K} 2^{-K} Z_n^K,$$

where D is a rather complicated sum of correction terms of the form $V_{2n-1} \otimes V_{2n} - V_{2n} \otimes V_{2n-1}$, but does not depend on any of the Z_n^K (that is not to say it is independent of them, just doesn't contain them).

27

Since Chen's relation holds for $(A_{0,1}, W_1)$, we can perform the same procedure with independent random variables $(A_{0,1}^K(n), W_1^K(n))$ (we omit the subscripts $_{0,1}$ and $_1$ when there is no ambiguity) and obtain

$$A^0 = D' + \sum_{n=1}^{2^K} 2^{-K} A^K(n).$$

where D' is again a weighted sum of the $W^K(n)$.

Now introduce the coupling γ:

1) $W^K(n) = V_n^K$ for all $n = 1, \ldots, 2^K$ (this is possible, since by definition $W^K(n)$ and V_n^K have the same marginals).

2) For any fixed n, the dependence between $A^K(n)$ and Z_n^K is unspecified, except that they both depend on V_n^K (but so far it is unknown whether the marginals of $A^K(n)$ and Z_n^K are equal).

3) The tuples $\left\{ \left(A^K(n), Z_n^K, V_n^K \right) : 1 \leq n \leq 2^K \right\}$ are independent.

Using this we can estimate the 2-Wasserstein distance

$$\left(\mathcal{W}_2(\mu, \nu) \right)^2 \leq \mathbb{E}_\gamma \left[\left\| (A^0, W^0) - (Z^0, V^0) \right\|_2^2 \right] = \mathbb{E}_\gamma \left[\left\| A^0 - Z^0 \right\|_2^2 \right]$$

$$= \mathbb{E}_\gamma \left[\left\| D' + \sum_{n=1}^{2^K} 2^{-K} A^K(n) \; - \; D + \sum_{n=1}^{2^K} 2^{-K} Z_n^K \right\|_2^2 \right]$$

$$= \mathbb{E}_\gamma \left[\left\| \sum_{n=1}^{2^K} 2^{-K} \left(A^K(n) - Z_n^K \right) \right\|_2^2 \right]$$

$$= \sum_{n=1}^{2^K} \mathbb{E}_\gamma \left[\left\| 2^{-K} \left(A^K(n) - Z_n^K \right) \right\|_2^2 \right]$$

$$= \sum_{n=1}^{2^K} 2^{-2K} \mathbb{E}_\gamma \left[\left\| A^K(n) - Z_n^K \right\|_2^2 \right]$$

$$\leq 2^{-K} \cdot 4 \max\{ \mathrm{var}(A^K(n)), \; \mathrm{var}(Z_n^K) \} = C \, 2^{-K},$$

where C is some finite constant independent of K.

Since $\mathcal{W}_2$ is a metric, this implies that $\mu = \nu$ as required. $\qquad\square$

We conclude this section with a result that heuristically says that the error between an estimator of Lévy area and the true distribution is bounded above by an explicit constant multiplied by the error between the estimator and one iteration of Chen-combine applied to the estimator. Let W be a d-dimensional Brownian motion and $A \in \mathbb{R}^{d \times d}$ be its associated Lévy area process. Let μ be a measure on $\mathbb{R}^d \times \mathbb{R}^{d \times d}$ and write $(X, Z) \sim \mu$ if for all $z \in \mathbb{R}^{d \times d}, x \in \mathbb{R}^d$ $\mathbb{P}(Z \in dz, X \in dx) = \mu(dz \times dx)$.

Theorem B.4 (Chen error bound). *Let W be a d-dimensional Brownian motion and $A \in \mathbb{R}^{d \times d}$ be its associated Lévy area process. Given a suitable square integrable, zero mean measure μ on $\mathbb{R}^d \times \mathbb{R}^{d \times d}$, define the "Lévy-error" of μ as*

$$\varepsilon_{L\acute{e}vy}^2 := \inf_{Z \in \Gamma} \mathbb{E}\left[\left\| Z - A_{0,1} \right\|_2^2 \right], \tag{20}$$

where Γ is the set of all random variables Z such that $(W_{0,1}, Z) \sim \mu$, and $\|\cdot\|_2$ is the usual l^2 norm defined on matrices. Let Z_1, Z_2 be independent random variables with distributions given

by $(\sqrt{2}W_{0,\frac{1}{2}}, Z_1) \sim \mu$ and $(\sqrt{2}W_{\frac{1}{2},1}, Z_2) \sim \mu$. *The assumed independence is possible by the independence of $W_{0,\frac{1}{2}}$ and $W_{\frac{1}{2},1}$. Write*

$$D := \left(W_{0,\frac{1}{2}} \otimes W_{\frac{1}{2},1} - W_{\frac{1}{2},1} \otimes W_{0,\frac{1}{2}}\right), \quad and \quad \widehat{Z} := \tfrac{1}{2}\left(Z_1 + Z_2 + D\right)$$

for the Chen-combine of Z_1 and Z_2. Using this, define the "Chen-error" as

$$\varepsilon_{Chen}^2 := \inf_{Z_3 \in \Gamma} \mathbb{E}\left[\left\|Z_3 - \widehat{Z}\right\|_2^2\right], \tag{21}$$

where Γ is the set of all random variables Z_3 such that $(Z_3, W_1) \sim \mu$. Then

$$\varepsilon_{L\acute{e}vy} \leq \left(2 + \sqrt{2}\right)\varepsilon_{Chen}. \tag{22}$$

Proof. Fix $\varepsilon > 0$, and since $W_1 \overset{d}{=} \sqrt{2}W_{0,\frac{1}{2}} \overset{d}{=} \sqrt{2}W_{\frac{1}{2},1}$ we can find random independent variables Z_1, Z_2 (possibly coupled to other random variables) with

$$\left(\sqrt{2}W_{0,\frac{1}{2}}, Z_1\right) \sim \mu \quad and \quad \left(\sqrt{2}W_{\frac{1}{2},1}, Z_2\right) \sim \mu$$

that satisfy

$$\mathbb{E}\left[\left\|Z_1 - 2A_{0,\frac{1}{2}}\right\|_2^2\right] \leq \varepsilon_{L\acute{e}vy}^2 + \varepsilon \quad and \quad \mathbb{E}\left[\left\|Z_2 - 2A_{\frac{1}{2},1}\right\|_2^2\right] \leq \varepsilon_{L\acute{e}vy}^2 + \varepsilon. \tag{23}$$

Similarly, let Z_3 be a random variable for which $(W_{0,1}, Z_3) \sim \mu$ and

$$\mathbb{E}\left[\left\|Z_3 - \widehat{Z}\right\|_2^2\right] \leq \varepsilon_{Chen}^2 + \varepsilon, \tag{24}$$

where $\widehat{Z}$ is defined as in the statement of the theorem and Z_1 and Z_2 being exactly those random variables satisfying the inequalities in Equation (23). Finally, recall by Chen's relation that $A_{0,1} = A_{0,\frac{1}{2}} + A_{\frac{1}{2},1} + \frac{1}{2}D$. With the joint random variable $\left(Z_1, Z_2, Z_3, A_{0,\frac{1}{2}}, A_{\frac{1}{2},1}, A_{0,1}, W_{0,\frac{1}{2}}, W_{\frac{1}{2},1}, W_{0,1}\right)$ now fully specified, we see that

$$\begin{aligned}
\varepsilon_{L\acute{e}vy}^2 &\leq \mathbb{E}\left[\left\|A_{0,1} - Z_3\right\|_2^2\right] \\
&= \mathbb{E}\left[\left\|A_{0,1} - \widehat{Z} - Z_3 + \widehat{Z}\right\|_2^2\right] \\
&\leq \mathbb{E}\left[\left\|A_{0,1} - \widehat{Z}\right\|_2^2\right] + \mathbb{E}\left[\left\|Z_3 - \widehat{Z}\right\|_2^2\right] - 2\mathbb{E}\left[\left\langle A_{0,1} - \widehat{Z}, \, Z_3 - \widehat{Z}\right\rangle\right].
\end{aligned}$$

The second term may be bounded as $\mathbb{E}\left[\left\|Z_3 - \widehat{Z}\right\|_2^2\right] \leq \varepsilon_{Chen}^2 + \varepsilon$. By construction

$$\begin{aligned}
A_{0,1} - \widehat{Z} &= A_{0,\frac{1}{2}} + A_{\frac{1}{2},1} + \frac{1}{2}D - \widehat{Z} \\
&= \left(A_{0,\frac{1}{2}} - \frac{1}{2}Z_1\right) + \left(A_{\frac{1}{2},1} - \frac{1}{2}Z_2\right),
\end{aligned}$$

allowing us to write

$$\begin{aligned}
\mathbb{E}\left[\left\|A_{0,1} - \widehat{Z}\right\|_2^2\right] &= \mathbb{E}\left[\left\|\left(A_{0,\frac{1}{2}} - \frac{1}{2}Z_1\right) + \left(A_{\frac{1}{2},1} - \frac{1}{2}Z_2\right)\right\|_2^2\right] \\
&= \frac{1}{4}\left(\mathbb{E}\left[\left\|Z_1 - 2A_{0,\frac{1}{2}}\right\|_2^2\right] + \mathbb{E}\left[\left\|Z_2 - 2A_{\frac{1}{2},1}\right\|_2^2\right]\right. \\
&\qquad\qquad \left. + \mathbb{E}\left[\left\langle Z_1 - 2A_{0,\frac{1}{2}}, \, Z_2 - 2A_{\frac{1}{2},1}\right\rangle\right]\right) \\
&\leq \frac{1}{2}\varepsilon_{L\acute{e}vy}^2 + \frac{1}{2}\varepsilon.
\end{aligned}$$

The cross terms vanish by independence and the mean zero property of all random variables involved. Finally we can bound the third term using the Cauchy-Schwarz inequality

$$-2\mathbb{E}\Big[\big\langle A_{0,1} - \widehat{Z}, \ Z_3 - \widehat{Z}\big\rangle\Big] \leq 2\mathbb{E}\Big[\big\|A_{0,1} - \widehat{Z}\big\|_2^2\Big]^{\frac{1}{2}}\mathbb{E}\Big[\big\|Z_3 - \widehat{Z}\big\|_2^2\Big]^{\frac{1}{2}}$$

$$\leq \sqrt{2}\big(\varepsilon_{\text{Lévy}}^2 + \varepsilon\big)^{\frac{1}{2}}\big(\varepsilon_{\text{Chen}}^2 + \varepsilon\big)^{\frac{1}{2}}$$

By substituting all bounds into the original inequality, and taking $\varepsilon \to 0$, we obtain

$$\varepsilon_{\text{Lévy}}^2 \leq \tfrac{1}{2}\varepsilon_{\text{Lévy}}^2 + \sqrt{2}\varepsilon_{\text{Lévy}}\varepsilon_{\text{Chen}} + \varepsilon_{\text{Chen}}^2 = \Big(\tfrac{1}{\sqrt{2}}\varepsilon_{\text{Lévy}} + \varepsilon_{\text{Chen}}\Big)^2.$$

Since all quantities are non-negative, we see that $\Big(1 - \tfrac{1}{\sqrt{2}}\Big)\varepsilon_{\text{Lévy}} \leq \varepsilon_{\text{Chen}}$ as required. $\qquad\square$

Lemma B.5. *Let W be a d-dimensional Brownian motion on $[0,1]$ and let B, H, b be the corresponding derived processes from Definition 3.1. Fix some $\xi \in \{-1,1\}^d$, and let H', and b' be the space-time and space-space Lévy area processes associated with the process $\xi \odot B = \{\xi \odot B_t\}_{t\in[0,t]}$, where $\odot$ denotes the Hadamard (coordinate-wise) product. Then*

$$\{B_t\}_{t\in[0,1]} \stackrel{d}{=} \{\xi \odot B_t\}_{t\in[0,1]}, \quad H' = \xi \odot H, \quad b' = (\xi \otimes \xi) \odot b, \quad \text{and} \quad (H', b') \stackrel{d}{=} (H, b).$$

Proof. By definition of H and b (in vector form)

$$H'_{0,t} = \frac{1}{t}\int_0^t \xi \odot B_{0,u}\,du = \xi \odot H_{0,t}$$

$$b'_{0,t} = \int_0^t (\xi \odot B_{0,u}) \otimes d(\xi \odot B_u)$$

$$= (\xi \otimes \xi) \odot \int_0^t B_{0,u} \otimes dB_u = (\xi \otimes \xi) \odot b_{0,t}.$$

$\qquad\square$

C Characteristic Function and Joint Moments

Here we briefly complete the definition of the joint characteristic function and Lévy area found in Theorem C.1, and also provide a proof of Proposition C.3. Part of the proof of the second result comes as a corollary of the form of the characteristic function found in Theorem C.1 and Lemma C.2.

Theorem C.1 (Characteristic function of Brownian motion and Lévy area). *Let $W_t = (W_t^{(1)}, \ldots W_t^{(d)})$ be a d-dimensional Brownian motion and let $A_t^{(j_1,j_2)}$ be the corresponding Lévy area of $W_t^{(j_1)}$ and $W_t^{(j_2)}$. Let $\mu \in \mathbb{R}^d$ and $\Lambda = \{\Lambda_{i,j}\}_{1\leq i<j\leq d} \in \mathbb{R}^{\frac{d(d-1)}{2}}$. The joint characteristic function of coupled Brownian motion W_t and the Lévy area A_t at time t*

$$\Phi_{(W,A)}(t, \mu, \Lambda) := \mathbb{E}\Bigg[\exp\Big(i\sum_{i=1}^d \mu_i W_{0,t}^{(i)} + i\sum_{1\leq j_1<j_2\leq d}\Lambda_{j_1,j_2}A_t^{(j_1,j_2)}\Big)\Bigg]$$

admits the following formula

$$\Phi_{(W,A)}(t, \mu, \Lambda) = \Bigg(\prod_{i=1}^{d_1}\frac{1}{\cosh(\frac{\eta_i}{2}t)}\Bigg)\exp\Bigg(\Big[\sum_{i=1}^{d_1}-\frac{1}{\eta_i}((R\mu)_{2i-1}^2$$

$$+ (R\mu)_{2i}^2)\tanh\Big(\frac{\eta_i}{2}t\Big)\Big] - \frac{1}{2}t\sum_{i=1}^{d_0}(R\mu)_{2d_1+i}^2\Bigg)$$

where R, η, d_0, d_1 are defined in Lemma C.2.

Proof. The result was first proved in [HS83] using a probabilistic approach. Recently, [LNT24] proposed a rough paths approach. $\qquad\square$

Lemma C.2 (Decomposition of anti-symmetric matrix). *For any $d \times d$ anti-symmetric real-valued matrix Λ, let $(\pm\eta_1 i, \ldots, \pm\eta_{d_1} i)$ be the set of non-zero conjugate eigenvalue pairs of Λ with $\eta_i > 0$ and $\eta_1 \geq, \ldots, \geq \eta_{d_1}$. Let $d_0 = d - 2d_1$ be the algebraic multiplicity of the eigenvalue 0 of Λ (if Λ does not have zero eigenvalues, then $d_0 = 0$). Then there exists an orthogonal matrix R, such that the following decomposition of Λ holds:*

$$\Lambda = R^T \Sigma R,$$

where Σ is in the form that

$$\Sigma = \begin{pmatrix} \Sigma_0, & \mathbf{0}_{d-d_0,d_0} \\ \mathbf{0}_{d_0,d-d_0} & \mathbf{0}_{d_0,d_0} \end{pmatrix}$$

$$:= \begin{pmatrix}
0 & -\eta_1 & 0 & 0 & \ldots & 0 & 0 & 0 & \ldots & 0 \\
\eta_1 & 0 & 0 & 0 & \ldots & 0 & 0 & 0 & \ldots & 0 \\
0 & 0 & 0 & -\eta_2 & \ldots & 0 & 0 & 0 & \ldots & 0 \\
0 & 0 & \eta_2 & 0 & \ldots & 0 & 0 & 0 & \ldots & 0 \\
\vdots & \vdots & \vdots & \vdots & \ddots & \vdots & \vdots & \vdots & \ldots & \vdots \\
0 & 0 & \ldots & 0 & \ldots & 0 & -\eta_{d_1} & 0 & \ldots & 0 \\
0 & 0 & \ldots & 0 & \ldots & \eta_{d_1} & 0 & 0 & \ldots & 0 \\
0 & 0 & \ldots & 0 & 0 & 0 & 0 & 0 & \ldots & 0 \\
0 & 0 & \ldots & 0 & 0 & 0 & 0 & \vdots & \ddots & \vdots \\
0 & 0 & \ldots & 0 & 0 & 0 & 0 & 0 & \ldots & 0
\end{pmatrix},$$

where Σ_0 is the block diagonal matrix with all non-zero η_i.

Proof. See [Gre81]. □

In the following proposition, we denote by $\mathbb{P}_{\mathrm{BF}}^{\theta,w}$ the output distribution of the BF generator given inputs w and θ, and the joint distribution of Brownian increments and fake area defined by the generator is denoted by $\mathbb{P}_{\mathrm{BF}}^{\theta}$.

Proposition C.3. *The following facts about the joint and conditional distributions of Brownian motion, Lévy area, and the BF generator hold.*

1) *If $r \sim \mathrm{Rad}\left(\frac{1}{2}\right)$ then $(rW_{0,t}, rA_{0,t}) \stackrel{d}{=} (W_{0,t}, rA_{0,t}) \stackrel{d}{=} (W_{0,t}, A_{0,t})$.*

2) *For any $n_i, n_{ij}, m_{ij} \in \mathbb{N}$, $1 \leq i < j \leq d$ it holds that*

$$\mathbb{E}_{(W_{0,1},A_{0,1})\sim\mathbb{P}_{(W_{0,1},A_{0,1})}}\left[\prod_{i=1}^d \left(W_{0,1}^{(i)}\right)^{n_i}\left(\prod_{1\leq i<j\leq d}\left(A_{0,1}^{(i,j)}\right)^{n_{ij}}\right)\right] = 0, \qquad (25)$$

$$\mathbb{E}_{(W_{0,1},\widetilde{A})\sim\mathbb{P}_{\mathrm{BF}}^{\theta}}\left[\prod_{i=1}^d \left(W^{(i)}\right)^{n_i}\left(\prod_{1\leq i<j\leq d}\left(\widetilde{A}^{(i,j)}\right)^{n_{ij}}\right)\right] = 0, \qquad (26)$$

$$\mathbb{E}_{A_{0,1}\sim\mathbb{P}_{A_{0,1}|W_{0,1}=w}}\left[\prod_{1\leq i<j\leq d}\left(A_{0,1}^{(i,j)}\right)^{m_{ij}}\right] = 0, \qquad (27)$$

$$\mathbb{E}_{\widetilde{A}\sim\mathbb{P}_{\mathrm{BF}}^{\theta,w}}\left[\prod_{1\leq i<j\leq d}\left(\widetilde{A}^{(i,j)}\right)^{m_{ij}}\right] = 0, \qquad (28)$$

provided that $\sum_{i=1}^d n_i + \left(\sum_{1\leq i<j\leq d} n_{ij}\right)$ and $\sum_{1\leq i<j\leq d} m_{ij}$ are odd.

Proof. To see item (1), fix $\mu \in \mathbb{R}^d$ and $\lambda = \{\lambda_{i,j}\}_{1\leq i<j\leq d} \in \mathbb{R}^{\frac{d(d-1)}{2}}$. We claim that

$$\Phi_{(W,\mathbf{A})}(t,\mu,\lambda) = \Phi_{(W,\mathbf{A})}(t,-\mu,-\lambda) = \Phi_{(W,\mathbf{A})}(t,\mu,-\lambda). \qquad (29)$$

Let Λ stand for the $d \times d$ anti-symmetric matrix with the above diagonal elements given by λ. Let Λ have a decomposition $\Lambda = R^T \Sigma R$ as in Lemma C.2. Then the corresponding decomposition for $-\Lambda$ is given by $\widetilde{R}^T \Sigma \widetilde{R}$, where for $1 \leq i \leq d_1$

$$\widetilde{R}_{2i,.} := R_{2i-1,.} \quad \text{and} \quad \widetilde{R}_{2i-1,.} := R_{2i,.}.$$

It is clear from the form of the characteristic function, that pairwise swapping the first $2d_1$ rows of R leaves the final value unchanged. Since all the terms involving μ are squared, the characteristic function is also invariant under taking the negative of μ. Item (1) now follows from Equation (29). For item (2), Equation (25) follows immediately from item (1), and Equation (27) follows from the fact that the conditional characteristic function of Lévy area given $W_{0,t} = \mathbf{w}$ is purely real [Wik01]. Equation (28) follows by independence of ξ_0 and the observation that its power will be odd. We finally turn our attention to Equation (26), where for simplicity we take $t = 1$. We recall that $\widetilde{A}_{0,1} \sim \mathbb{P}_{\mathrm{BF}}^{\theta}$ is defined by $\mathrm{BF}\left(W_{0,1}, H_{0,1}, \widetilde{b}_{0,1}, \xi, \boldsymbol{\xi}\right)$, where the only dependence is between $H_{0,1}$ and $\widetilde{b}_{0,1}$. Indeed, by expanding each $\widetilde{A}^{(i)}$ we see that it is enough to show that

$$\mathbb{E}\left[\prod_{i=1}^{d}\left(W^{(i)}\right)^{n_i}\left(\prod_{1 \leq i < j \leq d}(\xi_0)^{n_{ij}}\left(\xi_i H^{(i)} W^{(j)}\right)^{k_{ij}}\left(\xi_j H^{(j)} W^{(i)}\right)^{l_{ij}}\left(\xi_i \xi_j \widetilde{b}^{(i,j)}\right)^{p_{ij}}\right)\right] = 0, \quad (30)$$

where $k_{ij} + l_{ij} + p_{ij} = n_{ij}$. We consider three exhaustive, but overlapping cases.

i) $\sum_{1 \leq i < j \leq d} n_{ij}$ is odd.

ii) For some $1 \leq i \leq d$, the power of $W^{(i)}$ or ξ_i is odd.

iii) For every $1 \leq i \leq d$, the power of $W^{(i)}$ and ξ_i is even.

If i) holds, then the power of ξ_0 is odd and by independence Equation (30) is true. Item ii) is similar. To conclude, we will show that if iii) holds, then i) must also hold. We observe that the power of $W^{(i)}$ is given by

$$n_i + \sum_{1 \leq j < i} k_{ji} + \sum_{i < j \leq d} l_{ij},$$

and the power of ξ_i is given by

$$\sum_{1 \leq j < i} l_{ji} + p_{ji} + \sum_{i < j \leq d} k_{ij} + p_{ij}.$$

Under the assumption that all these powers are even, we may add them together to see that

$$\sum_{i=1}^{d} n_i + \left(\sum_{1 \leq j < i} k_{ji} + l_{ji} + p_{ji} + \sum_{i < j \leq d} k_{ij} + l_{ij} + p_{ij}\right) = \sum_{i=1}^{d} n_i + 2\left(\sum_{1 \leq i < j \leq d} n_{ij}\right)$$

is even. As the sum over all n_i and n_{ij} is odd by assumption, it must be the case that

$$\sum_{1 \leq i < j \leq d} n_{ij}$$

is odd. $\qquad \square$

D   Test metrics

We list in this section the test metrics we used to assess the performance of our generative model. Throughout the section let X, Y be d-dimensional random variables on the metric space (M, m) and let $\mu := \mathbb{P}_X$, $\nu := \mathbb{P}_Y$ be the induced probability measure. We denote by μ_i and ν_i the measure induced by the marginal distributions of $X^{(i)}$ and $Y^{(i)}$ respectively.

1) Marginal 2-Wasserstein metric. For $1 \leq i \leq d$, The 2-Wasserstein distance between $X^{(i)}$ and $Y^{(i)}$ is given by

$$\mathcal{W}_2(\mu, \nu) = \left(\inf_{\gamma \in \Gamma(\mu, \nu)} \int m(x, y)^2 \, d\gamma(x, y) \right)^{\frac{1}{2}}$$

where $\Gamma(\mu, \nu)$ is the set of all joint measures on $M \times M$ such that the marginal measure corresponds to μ and ν, i.e.

$$\int_M \gamma(x, y) \, dy = \mu(x)$$
$$\int_M \gamma(x, y) \, dx = \nu(y)$$

Wasserstein metric is a way of assessing the difference between two distributions, however, in practice the estimation is often intractable when d is high as it needs to compute $m(x, y)$ for all samples x and y. To accommodate this issue, we compute the $\mathcal{W}_2$ distance between the marginal distribution $X^{(i)}$ and $Y^{(i)}$ only.

2) Cross moment metric. We compare the difference of the fourth moments between the real and generated Lévy area. Let $\{\mathbf{X}_i\}_{i=1}^N$ be samples of the random variable X, for any $(i_1, i_2, i_3, i_4) \in \{1, \ldots, d\}^4$ we estimate the cross moment $\mathbb{E}[X^{(i_1)} X^{(i_2)} X^{(i_3)} X^{(i_4)}]$ by

$$\frac{1}{N^4} \sum_{1 \leq j_1, j_2, j_3, j_4 \leq N} \mathbf{X}_{j_1}^{(i_1)} \mathbf{X}_{j_2}^{(i_2)} \mathbf{X}_{j_3}^{(i_3)} \mathbf{X}_{j_4}^{(i_4)}$$

If X happens to be the Lévy area of Brownian motions we do know the analytical form of each cross-moment. One can derive it using the basic tools of rough path theory, i.e. the expected signature of Brownian motion. This metric is used to assess the joint fitting of generated Lévy area without using estimations of real data.

3) Characteristic Function Distance and Maximum Mean Discrepancy distance (MMD). In [Sri+10] it is shown that the characteristic function distance CFD_Λ when using an L^2 norm instead of an L^1 norm is equivalent to an MMD distance with a certain kernel. For example, if Λ is distributed as a Gaussian then the corresponding kernel is the Gaussian kernel. For our tests we use the MMD distance with both a Gaussian and polynomial kernel, with the Fourier series expansion with a high truncation level taken to be the ground truth.

4) Empirical Unitary Characteristic Function Distance. We parametrize the measure $\mathcal{M}$ on the space of linear transformations $\mathbb{R}^{d+a}$ onto $\mathfrak{g}_m$ by M linear maps, where d, a and m denotes the Brownian dimension, Lévy dimension, and unitary Lie degree respectively. Then, we train $\mathcal{M}$ to maximize the EUCFD distance between real and generated data. In practice, we set $m = 8$, $M = 128$, and train $\mathcal{M}$ for 2000 iterations, the EUCFD computed on an independent test set is used for model assessment.

E   Training procedure and hyperparameter tuning

We performed the training procedure as illustrated in Algorithm 4.

On the generator side, we used a FNN with 3 hidden layers and 16 hidden dimensions per layer. The activation function is chosen to be LeakyRelu with slope 0.01. The dimension of the noise vector is set to be 4.

On the discriminator side, we parameterize 128 linear maps onto the Lie algebra of degree 3 to mimic the empirical distribution used to compute UCFD mentioned in Section 4.1. The total number of training iterations is set to be 2500, where we observed the convergence on the marginal 2-Wasserstein metric on real data. We optimize both the generator and discriminator using Stochastic Gradient Descent and Adam optimizer. We set the batch size to 2^{13} and the learning rate for generator/discriminator is set to be 0.001/0.01 respectively. Both learning rates decay for each 500 iteration. Finally, we set iter_d to be 3.

Regarding the choice of some of the parameters, we have conducted a wide range hyperparameter grid search for training the LévyGAN. Tuning is done on both the generator and discriminator sides. The model selection is based on the marginal 2-Wasserstein metric. We provide here a complete grid for interested readers.

Hyperparameter	Grid values
Generator hidden layers	$2, 3, 5$
Generator hidden dimension	$8, 16$
Generator noise size	$4, 8$
Generator slope of LeakyRelu	$0.01, 0.2$
Discriminator Lie degree	$2, 3, 5$
Discriminator batch size	$16, 64, 128$

Table 5: Grid for hyperparameter tuning

F   Foster's Moment-Matching Method

Definition F.1 (Foster's approximation of Lévy area)**.** For any $0 \leq s < t$ and $d \geq 2$ we define the antisymmetric tensor $\widetilde{A}_{s,t}$ with entries

$$\widetilde{A}_{s,t}^{(i,j)} = H_{s,t}^{(i)} W_{s,t}^{(j)} - W_{s,t}^{(i)} H_{s,t}^{(j)} + 12 \Big(K_{s,t}^{(i)} H_{s,t}^{(j)} - H_{s,t}^{(i)} K_{s,t}^{(j)} \Big) + \widetilde{a}_{s,t}^{(i,j)}, \quad \text{for } 1 \leq i, j \leq d$$

where

- W is a d-dimensional Brownian motion and H is a space-time bridge Lévy area on $[s, t]$.

- $K_{s,t} \in \mathbb{R}^d$ is the space-time-time Lévy area of the Brownian bridge between s and t, is distributed as $K_{s,t} \sim \mathcal{N}^d\big(0, \frac{1}{720}(t - s)\big)$, with K and (W, H) being independent.

- $\widetilde{a}$ is an approximation of the Brownian arch Lévy area (see [Fos20], definition 4.1.14) constructed as shown below.

$$\widetilde{a}_{s,t}^{(i,j)} = \begin{cases} \sigma_{s,t}^{(i,j)} \xi_{s,t}^{(i,j)} & \text{if } i < j \\ -\sigma_{s,t}^{(i,j)} \xi_{s,t}^{(i,j)} & \text{if } j < i \\ 0 & \text{if } i = j \end{cases}$$

with the independent random variables $\sigma_{s,t}^{(i,j)}$ and $\xi_{s,t}^{(i,j)}$ defined for $1 \leq i < j \leq d$ according to

$$\xi_{s,t}^{(i,j)} \sim \begin{cases} \mathrm{Uni}\big[-\sqrt{3}, \sqrt{3}\big] & \text{with probability } p \\ \mathrm{Rad}(1/2) & \text{with probability } 1 - p \end{cases} \qquad \text{where } p := \frac{21130}{25621}$$

and

$$\sigma_{s,t}^{(i,j)} = \sqrt{\frac{3}{28} \big(C^{(i)} + c\big) \big(C^{(j)} + c\big) (t - s)^2 + \frac{1}{28}(t - s) \Big(\big(12 K_{s,t}^{(i)}\big)^2 + \big(12 K_{s,t}^{(i)}\big)^2 \Big)},$$

where the $C^{(i)} \sim \mathrm{Exp}\big(\frac{15}{8}\big)$, $(1 \leq i \leq d)$ are i.i.d. random variables and $c := \frac{1}{\sqrt{3}} - \frac{8}{15}$.

Theorem F.2. *Let $d \in \{2, 3\}$ and let $\widetilde{A}$ be as in Definition F.1. Then $\widetilde{A}$ matches all the fifth and lower moments of the Lévy area A conditional on W and H. That is, for any $n_1, n_2, n_3 \geq 0$ with $n_1 + n_2 + n_3 \leq 5$*

$$\mathbb{E}\left[\Big(\widetilde{A}_{s,t}^{(1,2)}\Big)^{n_1} \Big(\widetilde{A}_{s,t}^{(2,3)}\Big)^{n_2} \Big(\widetilde{A}_{s,t}^{(3,1)}\Big)^{n_3} \mid W_{s,t}, H_{s,t} \right] =$$

$$\mathbb{E}\left[\Big(A_{s,t}^{(1,2)}\Big)^{n_1} \Big(A_{s,t}^{(2,3)}\Big)^{n_2} \Big(A_{s,t}^{(3,1)}\Big)^{n_3} \mid W_{s,t}, H_{s,t} \right].$$

Proof. See [Fos20], page 190. □

G SDE Numerical Schemes

This section details the various numerical schemes with which we perform our tests. We start by recalling the definition of weak and strong errors and discuss why we are only able to analyse the former.

G.1 Weak vs Strong Error

Strong error measures the discrepancy between the true sample paths of the process and the approximate sample paths, while weak error measures the similarity between the distributions of the true and approximate solutions. Since our simulation methods are not exact, nor do they correspond to some approximation of a true sample of Lévy area (in comparison to a truncated Fourier series expansion for example), we cannot measure the strong error for schemes involving fake Lévy area. We can, however, measure the weak error of the discretisation schemes. Concretely, a discretisation scheme $\{\widehat{X}_k\}_{0 \leq k \leq N}$ is said to converge weakly with order α if for any polynomial p

$$\left| \mathbb{E}\big[p(\widehat{X}_N) - p(X_T) \big] \right| \leq C_p h^\alpha, \tag{31}$$

for some constant $C_p > 0$ and for all sufficiently small step sizes $h := \frac{T}{N}$. Convergence with weak order α will be denoted by $O(h^\alpha)$. The following subsections introduce three discretisation schemes that will be used for our numerical results.

G.2 Discretisation Schemes

Here we recall the definitions of the numerical schemes used for the results presented in Section 6.2.

G.2.1 Milstein's Method

Milstein's method is derived from the second order (Itô) Taylor expansion of the SDE in Equation (1). It is defined as follows: fix $N \geq 1$, set $\widehat{X}_0 = x_0$, and for all $0 \leq k \leq N - 1$ construct $\widehat{X}_{k+1}$ recursively via the relation

$$\begin{aligned}
\widehat{X}_{k+1} = {}& \widehat{X}_k + f(\widehat{X}_k)h + \sum_{i=1}^{d} g_i(\widehat{X}_k)\Delta W_k^{(i)} \\
& + \sum_{i,j=1}^{d} g_i'(\widehat{X}_k)g_j(\widehat{X}_k)\left(\frac{1}{2}(\Delta W_k^{(i)})(\Delta W_k^{(j)}) + A_k^{(i,j)} - \frac{1}{2}\delta_{ij}h \right),
\end{aligned} \tag{32}$$

where $h := \frac{T}{N}$, $\Delta W_k^{(i)} := W_{t_{k+1}}^{(i)} - W_{t_k}^{(i)}$, δ_{ij} is the Kronecker delta, and

$$A_k^{(i,j)} := \frac{1}{2}\left(\int_{t_k}^{t_{k+1}} (W_s^{(i)} - W_{t_k}^{(i)})dW_s^{(j)} - \int_{t_k}^{t_{k+1}} (W_s^{(j)} - W_{t_k}^{(j)})dW_s^{(i)} \right) \tag{33}$$

is the Lévy area. Milstein's method, under certain conditions, is known to converge with both weak and strong order $O(h)$. Meanwhile, removing the Lévy area terms leaves the weak order unchanged, but reduces the strong order to $O(\sqrt{h})$. Since we are concerned exclusively with weak convergence, we will consider Milstein's method without Lévy area.

G.2.2 Strang log-ODE

The Strang log-ODE method, introduced in [FRS24], is a higher order method that incorporates a term involving fake Lévy area. To define this scheme we must first convert the SDE in Equation (1) into Stratonovich form, that is

$$dX_t = \bar{f}(X_t dt + \sum_{i=1}^{d} g_i(X_t) \circ dW_t^{(i)}, \quad X_0 = x_0, \tag{34}$$

where the Stratonovich drift $\overline{f}$ is given by

$$\overline{f}(x) \coloneqq f(x) - \sum_{i=1}^{d} g_i'(x)g_i(x).$$

As in the Milstein scheme we fix $\widehat{X}_0 = x_0$, and recursively define

$$\widehat{X}_{k+1} = \exp\left(\tfrac{1}{2}h\overline{f}\right)\exp\left(\sum_{i=1}^{d} g_i\Delta W_k^{(i)} + \sum_{i<j}(g_j'g_i - g_jg_i')A_k^{(i,j)}\right)\exp\left(\tfrac{1}{2}h\overline{f}\right)\left(\widehat{X}_k\right), \quad (35)$$

where $\exp\left(Cf\right)(x)$ denotes the time 1 solution to the following ordinary differential equation

$$\frac{dy}{dt} = Cf(y), \ \ y_0 = x.$$

For the Lévy area term we will consider three different weak approximations: a Rademacher random variable which matches the variance of Lévy area, Foster's method, and our generative modelling method. The first method is based on the use of Rademacher random variables in Talay's scheme [Tal90].

G.3 Antithetic MLMC

Normally, in order to achieve optimal computational complexity of the MLMC it is required that the underlying discretisation scheme has strong order $O(h)$, see [Gil08], which requires strong simulation of Lévy area when the SDE is more than one dimensional. However, there exists clever reformulation of the standard MLMC which achieves optimal computational complexity using the no area Milstein scheme, despite only having a strong convergence rate of $O(\sqrt{h})$. Antithetic MLMC, proposed in [GS14], was originally motivated by the difficulty of simulating Lévy area exactly. Now, as mentioned in the previous subsection, on each level the coarse and fine path are generated using the same underlying Brownian motion. It is not in fact necessary to use the same estimator on both the coarse and fine paths. It suffices that $Y_l^{\cdot,l} \overset{d}{=} Y_l^{\cdot,l+1}$. For the antithetic method, the paper [GS14] uses two different paths on the fine level: the fine path itself and an antithetic twin. The antithetic twin is obtained by pairwise swapping the increments of the fine path; essentially this means that $\widehat{X}^{(f)} + \widehat{X}^{(a)} \approx 2\widehat{X}^{(c)}$, where $\widehat{X}^{(f)}$ denotes the fine path, $\widehat{X}^{(a)}$ the antithetic path, and $\widehat{X}^{(c)}$ the coarse path. The resulting effect is that the variance of $\frac{1}{2}(\varphi(\widehat{X}^{(f)}) + \varphi(\widehat{X}^{(a)})) - \varphi(\widehat{X}^{(c)})$ should be small. For more details, we refer the reader to [GS14].

G.4 The log-Heston SDE

We recall the definition of the log-Heston model as the following two-dimensional SDE

$$dU_t = \left(r - \frac{1}{2}V_t\right)dt + \sqrt{V_t}dW_t^{(1)}, \ \ U_0 \in \mathbb{R}$$
$$dV_t = \kappa(\theta - V_t)dt + \sigma\sqrt{V_t}dW_t^{(2)}, \ \ V_0 > 0. \tag{36}$$

The discounted payoff of a European call option for a price S with $d\log(S) \coloneqq U$ is

$$\varphi(S) \coloneqq e^{-rT}\left(e^{U_T} - K\right)^+.$$

The price at $t = 0$ of this option may be written as

$$C_0 \coloneqq \mathbb{E}\left[\varphi(S)\right] = S_0\Pi_0 - e^{-rT}K\Pi_1, \tag{37}$$

where the factors Π_0 and Π_1 area given by

$$\Pi_0 = \frac{1}{2} + \frac{1}{\pi}\int_0^\infty \mathfrak{R}\left[\frac{e^{i\omega K}\Psi_{U_T}(\omega - i)}{i\omega\Psi_{U_T}(-i)}\right]d\omega$$
$$\Pi_1 = \frac{1}{2} + \frac{1}{\pi}\int_0^\infty \mathfrak{R}\left[\frac{e^{i\omega K}\Psi_{U_T}(\omega)}{i\omega}\right]d\omega. \tag{38}$$

Here $\Psi_{\log Y_T}$ denotes the characteristic function of U_T. The characteristic function itself has an analytic form given by

$$\Psi_{U_T}(\omega) = \exp\left\{C(\omega)\theta + D(\omega)V_0 + i\omega \log\left(S_0 e^{rT}\right)\right\},$$

where the functions $C(\cdot)$ and $D(\cdot)$ are defined as

$$C(\omega) := \kappa\left[b_1 T - \frac{2}{\sigma^2}\log\left(\frac{1 - b_2 e^{-aT}}{1 - b_2}\right)\right]$$

$$D(\omega) := b_1 \frac{1 - e^{-at}}{1 - b_2 e^{-at}},$$

with constants a, b_1 and b_2 given by

$$a := \sqrt{\kappa^2 + \sigma^2\omega(\omega - i)}$$

$$b_1 := \frac{\kappa - a}{\sigma^2}$$

$$b_2 := \frac{\kappa - a}{\kappa_a}.$$

For full details of the derivation of this formula, we refer the reader to [Cri15]. While the preceding expression may appear complicated, it requires only the evaluation of the deterministic integrals in Equation (38), which are computed in practice using quadrature.

What remains to full specify the numerical schemes is to compute the one step recursion for the various numerical schemes applied log-Heston SDE from Equation (36). Full details and derivations of the vector field derivatives can be found in [Ter22]. The no-area Milstein update is given by

$$\widehat{U}_{k+1} = \widehat{U}_k + (r - \tfrac{1}{2}\widehat{V}_k)h + \sqrt{\widehat{V}_k}\Delta W_k^{(1)} + \tfrac{1}{4}\sigma\Delta W_k^{(1)}\Delta W_k^{(2)}$$

$$\widehat{V}_{k+1} = \widehat{V}_k + \kappa(\theta - \widehat{V}_n)h + \sigma\sqrt{\widehat{V}_k}\Delta W_k^{(2)} + \frac{1}{4}\sigma^2\left((\Delta W_k^{(2)})^2 - h\right). \tag{39}$$

The Strang log-ODE recursion is more involved as it involves solving two ordinary differential equations: one for the Stratonovich drift and one involving diffusion terms. Fortunately, these are analytically solvable, with the resulting scheme given by

$$\widetilde{V}_{k+1}^1 = (\widehat{V}_k + \xi)e^{-\frac{\kappa h}{2}} + \xi$$

$$\widetilde{U}_{k+1}^1 = \widehat{U}_k + \frac{1}{2\kappa}(\widehat{V}_k - \xi)(e^{-\frac{\kappa h}{2}} - 1) + \frac{h}{2}(r - \frac{\xi}{2}) \tag{40}$$

$$\widetilde{V}_{k+1}^2 = \left(\sqrt{\widetilde{V}_{k+1}^1} + \frac{\sigma}{2}\Delta W_k^{(2)}\right)^2$$

$$\widetilde{U}_{k+1}^2 = \widetilde{U}_{k+1}^1 + \sqrt{\widetilde{V}_{k+1}^1}\Delta W_k^{(1)} + \frac{\sigma}{4}\Delta W_k^{(1)}\Delta W_k^{(2)} - \frac{\sigma}{2}\widetilde{A}_k^{(1,2)}$$

$$\widehat{V}_{k+1} = (\widetilde{V}_{k+1}^2 - \xi)e^{-\frac{\kappa h}{2}} + \xi$$

$$\widehat{U}_{k+1} = \widetilde{U}_{k+1} + \frac{1}{2\kappa}(\widetilde{V}_{k+1}^2 - \xi)(e^{-\frac{\kappa h}{2}} - 1) + \frac{h}{2}(r - \frac{\xi}{2}),$$

where $\xi := \theta - \frac{\sigma^2}{4\kappa}$ and $\widetilde{A}$ denotes the fake Lévy area.